Article
Vol. 24, No. 6, p. 633–649, December 2020
https://doi.org/10.1007/s12303-020-0004-0
pISSN 1226-4806 eISSN 1598-7477
Geosciences Journal GJ

Geochemistry, zircon U-Pb ages and Sr-Nd-Hf isotopes of an Early Triassic appinitic complex in southeastern Inner Mongolia, China: implications for the late tectonic evolution of the Paleo-Asian Ocean

Junbin Zhu[1]* and Sumei Zhang[2]

[1]Institute of Geology, Chinese Academy of Geological Sciences, Beijing 100037, China
[2]School of Nature Resources, Hebei GEO University, Shijiazhuang 050031, China

ABSTRACT: Appinite commonly occurs in convergent plate tectonic settings and thus can constrain the tectonic evolution of ancient orogens. Geochemical and geochronological analyses were carried out on a newly identified Early Triassic appinitic complex in southeastern Inner Mongolia in the eastern segment of the Central Asian Orogenic Belt. Petrographically, the Luotuochang complex can be divided into two zones: an outer zone of intermediate rocks and inner zone dominated by mafic rocks. A monzonite sample from the outer zone yielded weighted mean zircon $^{206}Pb/^{238}U$ ages of 246 ± 1.6 Ma, whereas the gabbro from the inner zone yielded an age of 243 ± 1.2 Ma. The inner zone mafic rocks have SiO_2 contents of 45.56 to 54.27 wt% with high MgO, Cr, Ni and Sr contents, elevated Ba/Nb, Ba/Zr, Rb/Y and Th/Zr, and low TiO_2, Nb/Zr and Nb/Y. These features suggest that the metasomatized lithospheric mantle is the primitive magma source. SiO_2 contents of the outer zone intermediate rocks range from 57.6 to 63.69 wt% and K_2O, Ba and Sr contents are enriched; the $\varepsilon_{Nd}(t)$ (+2.2 to +4.0) and $\varepsilon_{Hf}(t)$ (+8.4 to +13.5) values are also high. These characteristics suggest that the magma of these rocks mainly derived from the mantle with possible juvenile lower crust involvement. Based on these geochemical data and results from regional geological investigations, we propose that the Luotuochang appinitic complex was formed in a post-orogenic extensional setting. Its formation was likely the result of lithospheric delamination, upwelling of new mantle material and partial melting of the overlying lower crust during crustal compression and thickening soon after the closure of the restricted Paleo-Asian Ocean basin.

Key words: Early Triassic, appinitic complex, petrogenesis, southeastern Inner Mongolia, Central Asian Orogenic Belt

Manuscript received August 5, 2019; Manuscript accepted January 13, 2020

1. INTRODUCTION

The Central Asian Orogenic Belt (CAOB), also known as the Altaid Tectonic Collage, extends from the Ural Mountains in the west to eastern Siberia in the east and from the Siberian craton in the north to the Tarim and North China cratons in the south (Sengör et al., 1993; Xiao et al., 2003; Windley et al., 2007). It is characterized by multiple Paleozoic accretionary, collisional processes of terranes, micro-continents, island arcs, seamounts and ophiolites as well as intra-continental deformation during the closure the Paleo-Asian Ocean (PAO) (Khain et al., 2002; Xiao et al., 2003, 2009, 2015; Li et al., 2016).

At present, it is generally agreed that the Solonker suture zone represents the final closure of the PAO as a result of collision and suturing between the North China and Siberian cratons. However, the tectonic evolution of the Solonker suture zone, especially the timing of the collision and suturing remains controversial, ranging from the middle–late Devonian (Tang et al., 1990; Xu and Chen, 1997; Xu et al., 2013), late Devonian to early Carboniferous (Shao, 1991) and the late Permian to Early–Middle Triassic (Xiao et al., 2003, 2009, 2015; Li, 2006; Chen et al., 2009). This uncertainty stems mainly from difficulties in identifying and correlating accretionary complexes and sedimentary successions along the suture that are intensively disrupted by post-Paleozoic tectonic movement. Moreover, the geochronology of the ophiolite mélanges,

*Corresponding author:
Junbin Zhu
Institute of Geology, Chinese Academy of Geological Sciences, No. 26, Baiwanzhuang Street, Beijing 100037, China
Tel: +86-13522602733, Fax: +86-10-68999662,
E-mail: zhujunbin0819@163.com

with estimated ages ranging from early Paleozoic to late Mesozoic (Liang, 1994; Wang and Fan, 1997; Miao et al., 2007; Jian et al., 2010), makes it hard to constrain the final closure of the PAO.

Fortunately, we recently have identified a new Triassic appinitic complex near the Solonker suture zone. An appinitic complex is typically dominated by mafic and intermediate rocks with indicative mineralogical and textural features for water-rich magmas. Their geochemistry commonly shows calc-alkaline to shoshonitic affinities (Fowler, 1988; Atherton and Ghani, 2002; Castro et al., 2003; Yuan et al., 2016). Moreover, what is particularly remarkable for appinitic rocks is their close spatiotemporal and genetic connections with critical geodynamic processes, such as arc-continental or continental-continental collisions, post-subduction slab break-off or delamination during the latest stage of an orogeny (Atherton and Ghani, 2002; Zhang et al., 2012; Murphy, 2013). Therefore, constraining the origin and tectonic setting of appinitic rocks can provide important information for describing the tectonic evolution of an ancient orogenic belt.

In this study, new zircon U-Pb ages and in situ zircon Hf isotopic data, whole-rock Sr-Nd isotopes and major and trace element compositions of different rocks in the complex are presented to constrain the sources and petrogenesis of the intrusions and describe the geodynamic environment during their emplacement. Results from such studies can lead to further insight into the transformation of the eastern segment of the CAOB from collision to post-collision. By integrating the results of this study with previously reported Paleozoic magmatic data in the region, these data can be further used to constrain the evolution of the late tectonic stage of the eastern segment of the CAOB.

2. GEOLOGICAL BACKGROUND

Southeastern Inner Mongolia, located in the eastern segment of the CAOB, is regarded as the area of final closure of the PAO (Fig. 1). There are five major E-W trending geological units in this region, from north to south: the Uliastai continental margin, the Northern Orogenic Belt (NOB), the Solonker suture zone, the Southern Orogenic Belt (SOB) and the North China Craton (NCC) (Xiao et al., 2003; Jian et al., 2010; Xu et al., 2013). The basement of the Uliastai continental margin is composed of

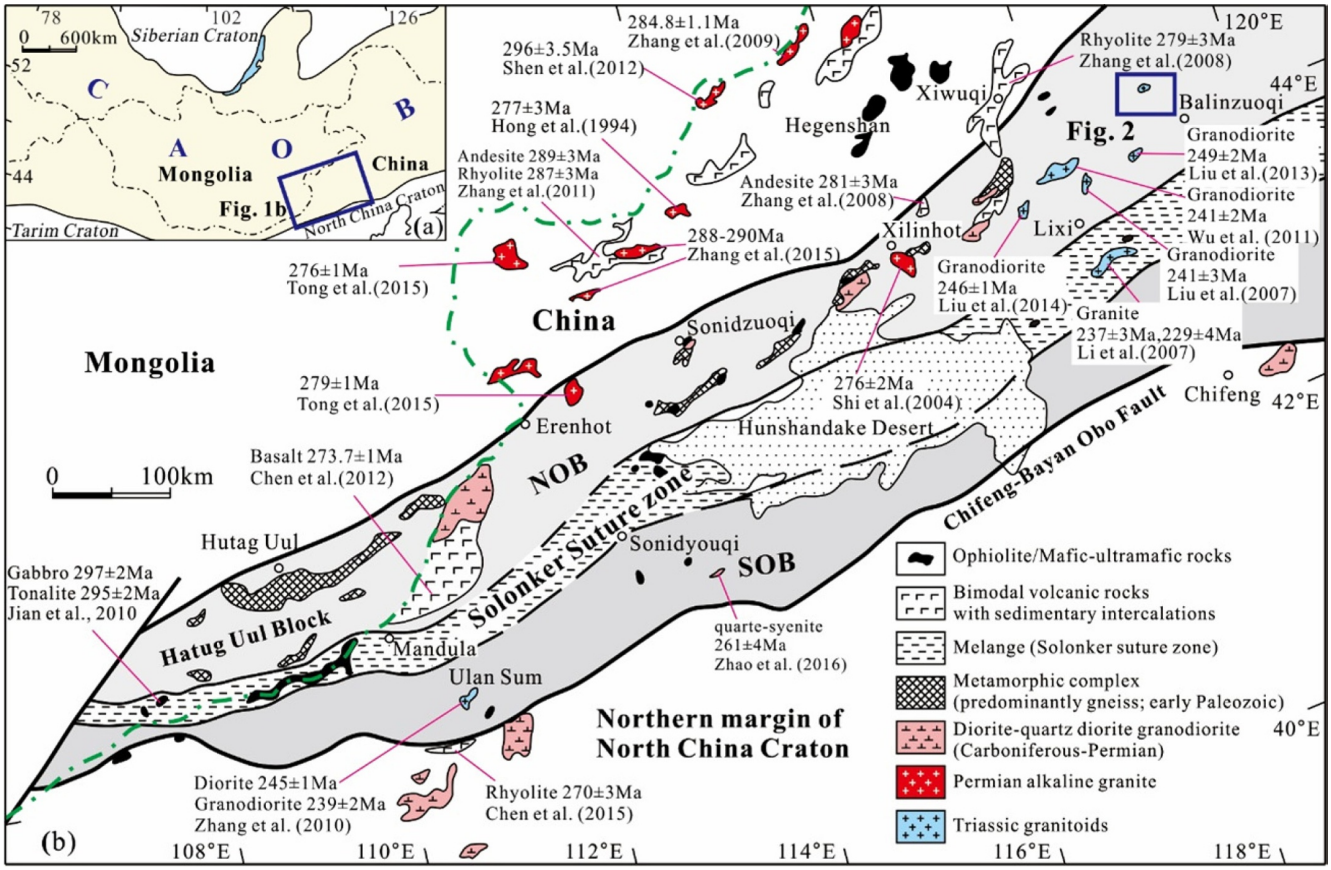

Fig. 1. (a) Simplified geological map of the Central Asian Orogenic Belt (CAOB) and the location of the studied area (modified after Jahn et al., 2004). (b) Simplified tectonic map of the southeastern CAOB showing the main tectonic subdivisions and the location of Figure 2 (modified after Xiao et al., 2003; Jian et al., 2010). The light gray zone represents the early–middle Paleozoic Northern Orogenic Belt (NOB), whereas the dark gray zone represents the early–middle Paleozoic Southern Orogenic Belt (SOB). Published zircon U-Pb ages are from Hong et al. (1994), Shi et al. (2004), Zhang et al. (2008, 2011, 2015), Jian et al. (2010), Chen et al. (2012, 2015), Liu et al. (2013, 2014), and Tong et al. (2015).

Proterozoic to Cambrian basement and overlain by late Paleozoic to Mesozoic rocks. There is also an exposure of an early–middle Permian NEE-trending alkaline granitic belt (292–275 Ma) associated with bimodal volcanic rocks (298–271 Ma), which are thought to have been formed in an extensional setting (Hong et al., 1994; Zhang et al., 2008; Li et al., 2015; Tong et al., 2015). The NOB consists mainly of the Precambrian Xilinhot metamorphic complex, the Devonian Erdaojing subduction-accretion complex and Paleozoic to Mesozoic volcano-sedimentary sequences. The Xilinhot metamorphic complex consists of schist, gneiss, amphibolite and ultramafic rocks. The isolated blocks of metamorphic rocks are interpreted as continental fragments incorporated into the subduction-accretion complex prior to the formation of the Solonker suture zone (Xiao et al., 2003; Jian et al., 2010). The Solonker suture zone, extending from Solonker to Linxi via Sonidyouqi, is considered the site of final PAO closure and records the terminal evolution of the CAOB in Inner Mongolia (Li, 2006). This suture zone contains abundant ophiolite fragments roughly along the Xar Moron River, such as the Kedanshan, Jiujingzi and Xingshuwa ophiolitic mélanges. Permian radiolarian fossils were found in the Xingshuwa ophiolitic mélange (Wang and Fan, 1997), which marks the suture of the eastern segment of the PAO (Xiao et al., 2003, 2009). The southern part of the Solonker suture zone consists of two tectonic units, the NCC and SOB, which are separated by the E-W-trending Bayan Obo–Chifeng fault zone. The SOB (also known as the Ondor Sum–Wengniute Orogenic Belt) is composed of the Ondor Sum complex with blueschist, SSZ-type ophiolitic mélange (approximately 497–477 Ma) and the Bainaimiao arc chain (approximately 488–438 Ma) (Jian et al., 2008; Zhang et al., 2014). These rock units are unconformably overlain by late Silurian–earliest Devonian Xibiehe Formation continental molasse deposits or Carboniferous and Permian volcano-sedimentary sequences. The NCC is characterized by highly metamorphosed Archean and Proterozoic basement.

The study area is situated in the NOB. It mainly features a series of Paleozoic to Mesozoic volcano-sedimentary sequences and episodic late Paleozoic to Mesozoic intrusions. The outcropping strata around the Luotuochang complex include early Permian Dashizhai Formation volcano-sedimentary sequences, middle Permian Zhesi Formation clastic deposits and late Permian Linxi Formation clastic rocks. The marine Dashizhai Formation consists mainly of mafic lava, tuff and volcaniclastic rocks, and the Zhesi Formation is dominated by sandstone, limestone and conglomerate. The continental facies of the Linxi Formation is typically composed of dark gray siltstone, shale and slate.

3. FIELD RELATION AND PETROGRAPHY

The Triassic Luotuochang complex, with an outcropping area of ~12 km^2, intrudes into Permian sedimentary and volcanic rocks. External contacts of this complex with its host rocks are sharp, steep and generally marked by thermal aureoles. The complex consists of a wide variety of rock types ranging from gabbro through monzodiorite and monzonite to quartz monzonite. Petrographically, the more mafic rocks of the Luotuochang complex are at the center, surrounded by monzonite and monzodiorites. Thus, the complex can be divided into two zones (Fig. 2): an outer zone of intermediate rocks and an inner zone dominated by mafic rocks with few ultramafic rocks. The contacts among the different rock units are transitional.

The rock association of the outer zone mainly comprises medium- to fine-grained monzonites and quartz monzonites that have subhedral granular textures and massive structures (Figs. 3c and d). Light gray quartz monzonites have euhedral to subhedral plagioclase (50–55%), subhedral alkali feldspar (20%), anhedral quartz (10–15%), amphibole (5%) and minor amounts of biotite (< 5%) with accessory apatite, zircon and Fe-oxide.

The inner zone is predominantly composed of medium- to fine-grained gabbrodiorite and gabbro with minor amounts of monzodiorite and olivine-gabbro (Figs. 3a and b). The mineralogical composition of the gabbrodiorite is dominated by plagioclase (60–65%), followed by hornblende (15–25%), alkali feldspar (< 5%) and accessory minerals, including apatite and zircon. The hornblende is a relic of the uralitization of augite. The gabbro mainly consists of plagioclase (55–70%), clinopyroxene (10–25%), hornblende (3%) and biotite (2%). The plagioclase is subhedral to euhedral and 2–4 mm in length. The clinopyroxene commonly occurs as relics, variably replaced by hornblende (Figs. 3e and f).

A monzonite sample (14LTC4-1) from the outer zone and a gabbro sample (14LTC10-1) from the inner zone were selected for zircon U-Pb isotopic analyses. Six whole-rock samples were selected for Sr-Nd isotopic analyses and another 14 samples were chosen for whole-rock geochemical analyses (Fig. 2).

4. ANALYTICAL METHODS

4.1. Zircon U-Pb Analyses

Zircons were extracted from whole-rock samples using standard techniques of density and magnetic separation at the Langfang Regional Geological Survey, Hebei Province, China. The separated zircons were mounted in epoxy resin and then were polished. After applying a gold coating onto the resin disk, cathodoluminescence (CL) images were collected using a Hitachi S3000N scanning electron microscope at the Beijing SHRIMP Center. Zircon U-Pb isotopic analysis was completed at the Isotope Laboratory of Tianjin Center, China Geological Survey. Zircon dating was conducted on Agilent 7500a inductively coupled plasma mass

https://doi.org/10.1007/s12303-020-0004-0

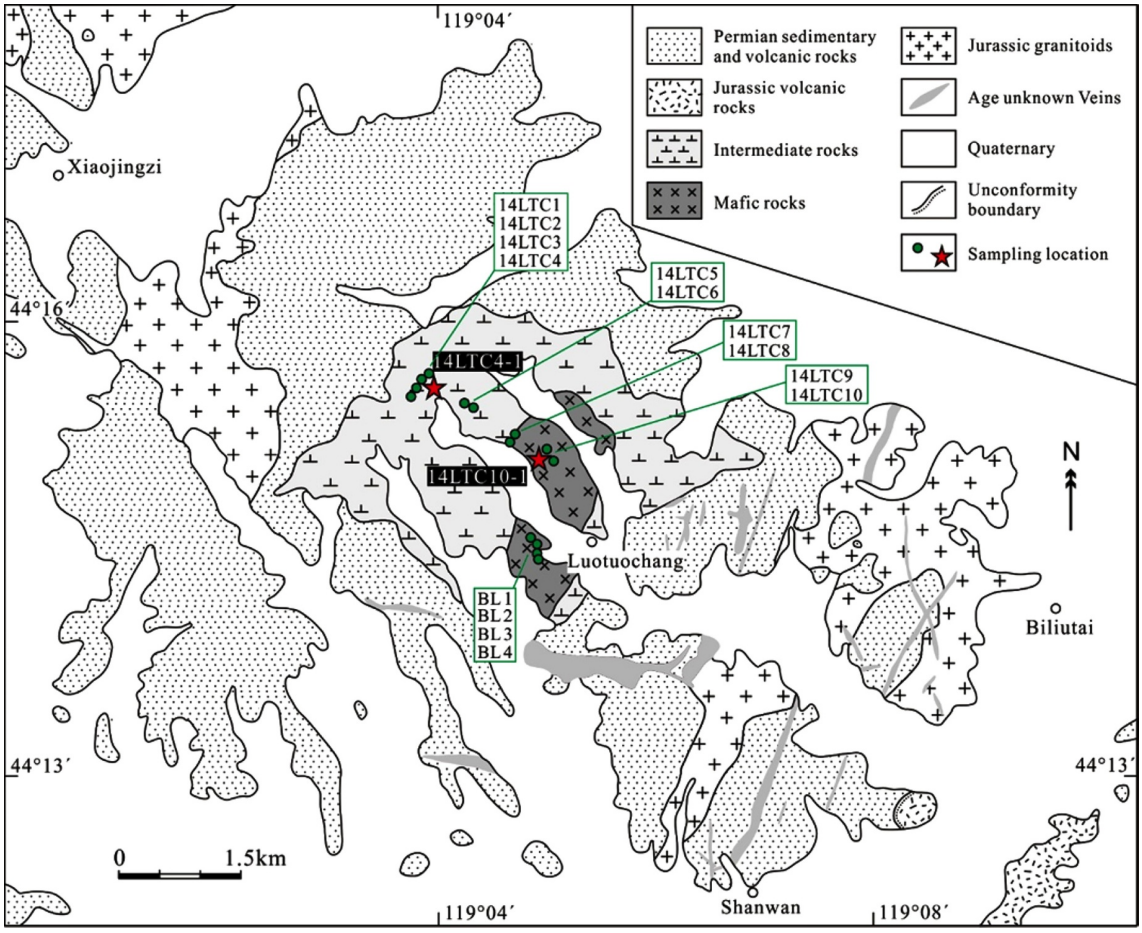

Fig. 2. Geological map of the Luotuochang complex, shown with the sample locations (modified from BGMRNM, 1985).

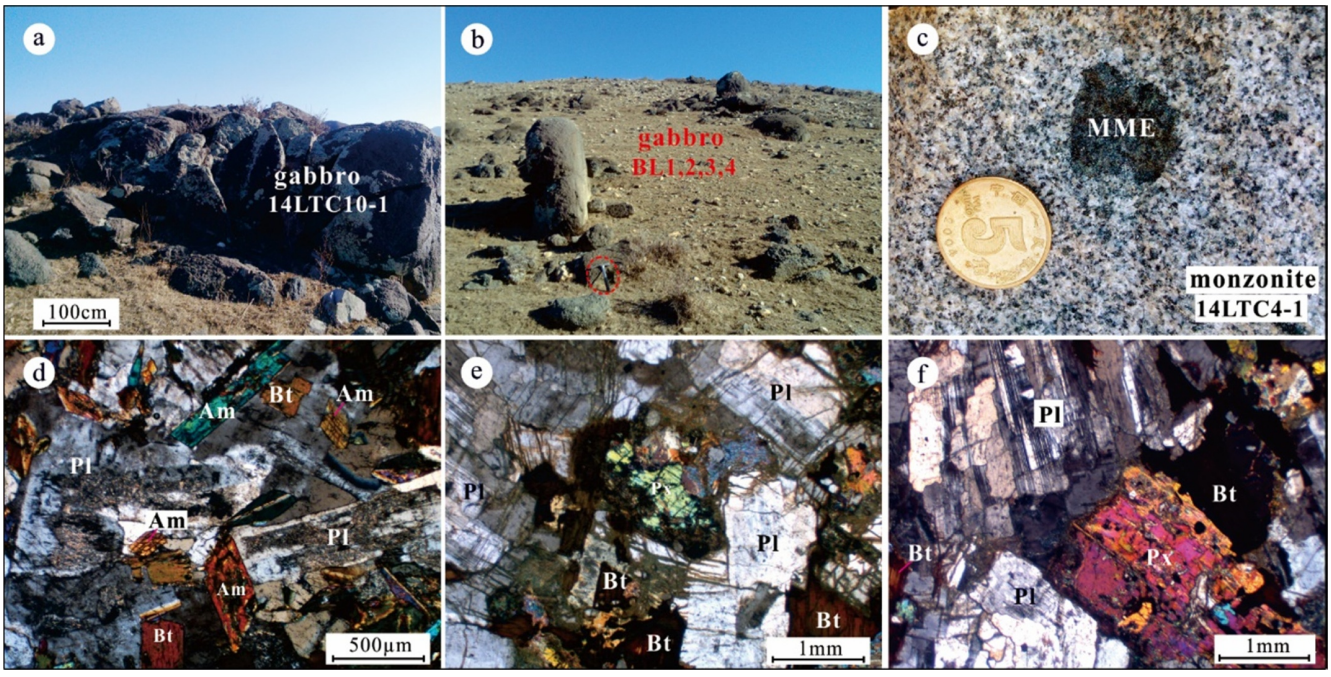

Fig. 3. Outcrop photographs and micrographs of the Luotuochang complex. (a) Field photograph of gabbro; (b) field photograph of gabbro; (c) field photograph of MME-bearing monzonite (The diameter of the coin is 2 cm); (d) photomicrograph of monzonite; (e) photomicrograph of gabbro; (f) photomicrograph of gabbro. Mineral abbreviations: Bt, biotite; Pl, plagioclase; Am, Amphibole; Px, pyroxene.

spectrometer (ICP-MS) equipped with the New Wave 193 nm FX laser ablation system. The laser system delivered a beam of UV light (193 nm) from a frequency-quintupled Neptune instrument (Thermo Fisher Company). Analyses were carried out with a beam diameter of 35 μm, repetition rate of 8–10 Hz and energy of 10–11 J/cm^2. Data acquisition for each analysis was 20 s for the background and 40 s for the signal. Mass discrimination with the MS and residual elemental fractionation were corrected by calibration against a homogeneous zircon standard (TEMORA/GJ-1). Typical operating conditions of the ICP-MS in the experiment and detailed analytical procedures from Liu et al. (2008) were strictly followed. Off-line selection, background integration, analysis signals and time-drift correction and quantitative calibration were conducted with the in-house software (ICPMSDataCal) (Liu et al., 2008). Common Pb corrections were processed with non-radiogenic ^{204}Pb, following the method of Andersen (2002), and used an average present-day crustal composition (Stacey and Kramers, 1975) as the common Pb which was assumed to be introduced mainly from surface contamination or the gold coating during sample preparation. Concordia diagrams and age calculations were made using Isoplot (v 3.0) (Ludwig, 2003). Analytical data of the Luotuochang complex are listed in Table 1.

4.2. Zircon Hf Isotopic Analyses

Zircon Hf isotope analysis was carried out in situ using a New Wave Research UP193FX laser-ablation microprobe, attached to a Neptune multicollector ICP-MS at the Isotope Laboratory

Table 1. Zircon U-Pb data of the Luotuochang complex from Balinzuoqi area, Inner Mongolia

Spot no.	Pb (ppm)	U (ppm)	^{232}Th/^{238}U	Isotopic ratios						Ages (Ma)					
				^{206}Pb/^{238}U	1σ	^{207}Pb/^{235}U	1σ	^{207}Pb/^{206}Pb	1σ	^{206}Pb/^{238}U	1σ	^{207}Pb/^{235}U	1σ	^{207}Pb/^{206}Pb	1σ
Sample 14LTC4-1															
1	30	636	1.3847	0.0392	0.0004	0.2764	0.0038	0.0512	0.0007	248	2	248	3	248	30
2	24	526	1.3161	0.0382	0.0004	0.2715	0.0039	0.0515	0.0007	242	2	244	4	263	31
3	27	587	1.2957	0.0391	0.0004	0.2870	0.0039	0.0532	0.0007	247	2	256	3	337	28
4	12	282	0.9873	0.0386	0.0004	0.2819	0.0044	0.0529	0.0008	244	2	252	4	326	33
5	11	248	1.1556	0.0389	0.0004	0.2753	0.0050	0.0513	0.0009	246	2	247	4	255	40
6	6	156	0.4573	0.0391	0.0004	0.2777	0.0074	0.0514	0.0013	247	3	249	7	260	59
7	23	518	1.1636	0.0396	0.0004	0.2814	0.0041	0.0515	0.0007	250	2	252	4	265	32
8	14	325	1.0437	0.0388	0.0004	0.2733	0.0043	0.0511	0.0008	245	2	245	4	247	35
9	11	251	1.1302	0.0385	0.0004	0.2777	0.0111	0.0523	0.0018	244	2	249	10	300	80
10	15	370	0.4733	0.0395	0.0004	0.2828	0.0050	0.0520	0.0009	250	2	253	4	283	38
11	20	463	0.9693	0.0393	0.0004	0.2816	0.0051	0.0520	0.0009	248	2	252	5	284	39
12	23	533	1.2868	0.0384	0.0004	0.2798	0.0040	0.0528	0.0007	243	2	250	4	320	30
13	25	537	1.5828	0.0385	0.0004	0.3172	0.0055	0.0597	0.0009	244	2	280	5	593	32
14	13	304	1.1574	0.0380	0.0004	0.2704	0.0042	0.0516	0.0007	241	2	243	4	267	33
15	15	364	1.2634	0.0389	0.0004	0.2719	0.0042	0.0507	0.0007	246	2	244	4	227	34
16	23	543	1.5063	0.0386	0.0004	0.2720	0.0039	0.0512	0.0007	244	2	244	4	248	31
Sample 14LTC10-1															
1	15	360	0.9392	0.0386	0.0004	0.2804	0.0042	0.0527	0.0007	244	2	251	4	317	32
2	37	873	1.1438	0.0383	0.0004	0.2692	0.0037	0.0510	0.0006	242	2	242	3	240	29
3	19	454	0.9393	0.0389	0.0004	0.2726	0.0039	0.0509	0.0007	246	2	245	4	235	31
4	33	777	0.9496	0.0386	0.0004	0.2711	0.0038	0.0509	0.0006	244	2	244	3	237	29
5	11	264	1.0613	0.0387	0.0004	0.2796	0.0049	0.0524	0.0009	245	2	250	4	302	38
6	12	289	0.6653	0.0384	0.0004	0.2807	0.0042	0.0530	0.0008	243	2	251	4	330	32
7	12	291	0.8762	0.0381	0.0004	0.2687	0.0043	0.0511	0.0008	241	2	242	4	245	35
8	8	181	0.9973	0.0387	0.0004	0.2839	0.0053	0.0531	0.0009	245	2	254	5	335	40
9	19	437	1.1054	0.0386	0.0004	0.2811	0.0041	0.0529	0.0007	244	2	252	4	323	31
10	8	195	0.8307	0.0389	0.0004	0.2734	0.0052	0.0510	0.0009	246	2	245	5	242	42
11	19	426	1.0295	0.0380	0.0004	0.2746	0.0043	0.0524	0.0008	240	2	246	4	304	33
12	6	154	0.7559	0.0383	0.0004	0.2734	0.0058	0.0519	0.0011	242	2	245	5	280	48
13	10	242	0.8798	0.0384	0.0004	0.2801	0.0046	0.0530	0.0008	243	2	251	4	328	36
14	9	210	1.0602	0.0382	0.0004	0.2699	0.0050	0.0513	0.0009	241	2	243	5	254	41
15	7	168	0.9210	0.0384	0.0004	0.2744	0.0056	0.0519	0.0010	243	2	246	5	283	46

https://doi.org/10.1007/s12303-020-0004-0

of Tianjin Center, China Geological Survey. Analyses were performed with an ablation pit 50 μm in diameter repetition rate of 10 Hz, ablation time of 60 s and a laser beam energy of 0.155 mJ per pulse. The measured isotopic ratios of $^{176}Hf/^{177}Hf$ were normalized to a $^{179}Hf/^{177}Hf$ value of 0.7325 for mass bias. The isobaric interferences of ^{176}Lu and ^{176}Yb on ^{176}Hf are monitored by the ratios of $^{176}Lu/^{175}Lu$ (= 0.02655) and $^{176}Yb/^{172}Yb$ (= 0.5887) obtained on the same spot during Hf analysis. Detailed instrument operation parameters, analytical procedures and data processing are similar to Geng et al. (2011). A zircon sample (GJ-1) was used as the reference standard and was analyzed twice before and after every eight analyses of unknown materials. Repeated GJ-1 measurements yielded weighted mean $^{176}Hf/^{177}Hf$ ratios of 0.282003 ± 31 (2 SD, n = 31), which is identical to previously reported values (Geng et al., 2011). The measured $^{176}Hf/^{177}Hf$ ratios and the ^{176}Lu decay constant ($1.865 \times 10^{-11} yr^{-1}$) were used to calculate initial $^{176}Hf/^{177}Hf$ values (Scherer et al., 2001). The $\varepsilon_{Hf}(t)$ values were calculated from chondritic values of $^{176}Hf/^{177}Hf$ (= 0.282772) and $^{176}Lu/^{177}Hf$ (= 0.0332) (Blichert-Toft and Albared, 1997). The depleted-mantle Hf model age (T_{DM1}) was calculated with present-day $^{176}Hf/^{177}Hf$ (0.28325) and $^{176}Lu/^{177}Lu$ (0.0384) values (Griffin et al., 2000).

4.3. Whole-rock Geochemical Analyses

Whole-rock geochemical analyses were performed at the Analytical Laboratory, Beijing Institute of Uranium Geology, China. Major elements were analyzed by X-ray fluorescence spectrometry with a Phillips PW 2404 system using the methods of Norrish and Hutton (1969). Ferrous iron was determined by the wet chemical titration method. For trace elements analyses, whole-rock powers (40 mg) were dissolved in distilled HF + HNO_3 in high-pressure Teflon bombs at 190 °C for 2 days. Samples were then evaporated to dryness, 1 ml of HNO_3 was added and the sample was dried twice before re-dissolution in HNO_3. Dissolved samples were diluted with 1% HNO_3 to 49 ml and 1 ml of 500 ppb indium was added as an internal standard. Trace elements, including rare earth elements (REEs) were determined by ICP-MS (Finnigan MAT Element I) following Liang and Gregoire (2000). A blank solution was prepared and the total procedural blank indicated < 50 ng for all trace elements. The analytical uncertainty for major elements was generally within 1–5%. In-run analytical precision for most trace elements was better than 5%.

4.4. Whole-rock Sr-Nd Analyses

The Rb-Sr and Sm-Nd isotopic compositions were measured at the Analytical Laboratory, Beijing Institute of Uranium Geology, China, using an ISOPROBE-T and Phoenix thermal ionization mass spectrometers, respectively. Detailed chemical separation and isotopic measurement procedures were similar to Wu et al. (2005). The precision for Rb, Sr, Sm, Nd, $^{87}Rb/^{86}Sr$ and $^{147}Sm/^{144}Nd$ was ±0.2% (2σ), and the precision for $^{87}Sr/^{86}Sr$ and $^{143}Nd/^{144}Nd$ (2σ) is shown in Table 4. The $^{87}Sr/^{86}Sr$ were normalized to an $^{86}Sr/^{88}Sr$ value of 0.1194 and $^{143}Nd/^{144}Nd$ were normalized to $^{146}Nd/^{144}Nd$ (= 0.7219). Total procedural blanks were < 300 pg for Sr and < 100 pg for Nd, and the estimated analytical uncertainties of $^{147}Sm/^{144}Nd$ and $^{87}Rb/^{86}Sr$ were < 0.5%. A Sr standard solution (NBS 987) was analyzed and yielded an $^{87}Sr/^{86}Sr$ of 0.710250 ± 14 (2σ), whereas the Nd standard solution (SHINESTU) yielded a ratio of 0.512113 ± 6 (2σ) during data acquisition. The United States Geological Survey reference material BCR-1 was measured as an unknown to monitor the accuracy of the analytical procedure. Measurements yielded $^{87}Sr/^{86}Sr$ of 0.705014 ± 3 (2σ) and $^{143}Nd/^{144}Nd$ of 0.512615 ± 12 (2σ).

5. ANALYTICAL RESULTS

5.1. Zircon U-Pb Ages

Zircons from the monzonite sample (14LCT4-1) are mostly prismatic and stubby in shape with lengths between 100 and 250 μm. In the CL images, most of them exhibit oscillatory zoning, indicative of a magmatic origin (Fig. 4). Sixteen analyses on 16 grains yielded U concentrations from 156 to 636 ppm, Th concentrations from 71 to 881 ppm and Th/U from 0.46 to 1.51. With the exception of one spot (grain 13), all of the zircons analyzed fall on or near the concordia line and yielded a weighted $^{206}Pb/^{238}U$ age of 246 ± 2 Ma (MSWD = 1.5), which was interpreted as the intrusion age.

Zircons from the gabbro sample (14LTC10-1) are subhedral and irregularly shaped grains 100–300 μm in length. Most zircons display oscillatory zoning without inherited cores or overgrowths (Fig. 4). A total of 15 zircons were analyzed and the U and Th contents are 154–873 ppm and 116–999 ppm, respectively. The Th/U from these samples range from 0.67 to 1.14. The data yielded a weighted mean $^{206}Pb/^{238}U$ age of 243 ± 1 Ma (MSWD = 0.5) (Fig. 5).

5.2. Whole-rock Major and Trace Elements

To characterize the geochemical variations within the Luotuochang complex, representative samples from each of the main rock types were analyzed for major and trace elements (Fig. 2; Table 2).

The rocks show a wide range in silica content from mafic compositions to intermediate (Fig. 6a). To simplify the descriptions, we classified all of the rocks into either the intermediate suite (outer zone rocks, $SiO_2 \geq 55$ wt%) or mafic suite (inner zone rocks, $SiO_2 < 55$ wt%). The mafic suite fell within gabbro, gabbroic

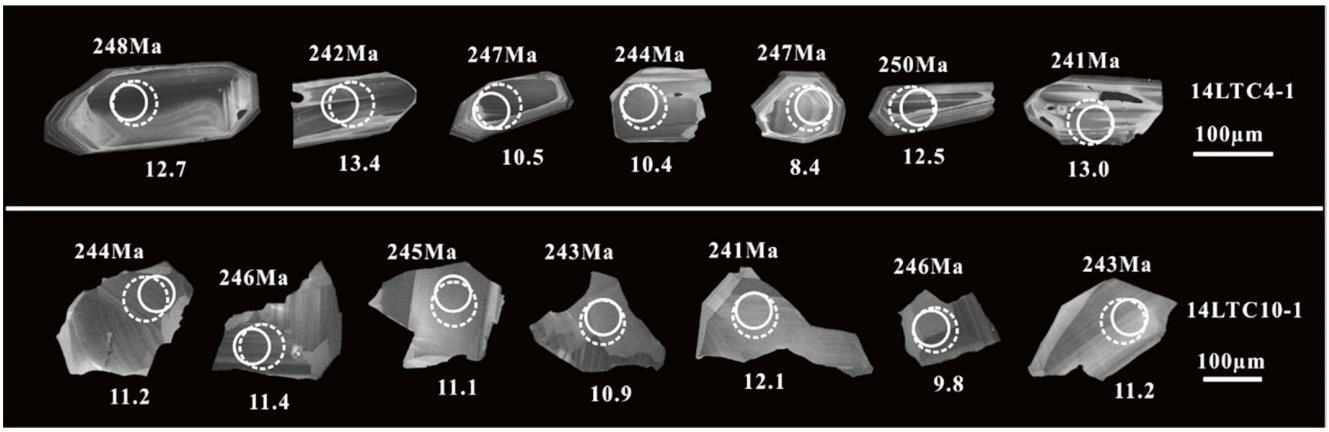

Fig. 4. Representative cathodoluminescence (CL) images of zircons from the Luotuochang complex. The solid-line circles show LA-ICP-MS dating spots and corresponding U-Pb ages, and the dashed-line circles show Lu-Hf isotope analysis spots and corresponding $\varepsilon_{Hf}(t)$ values.

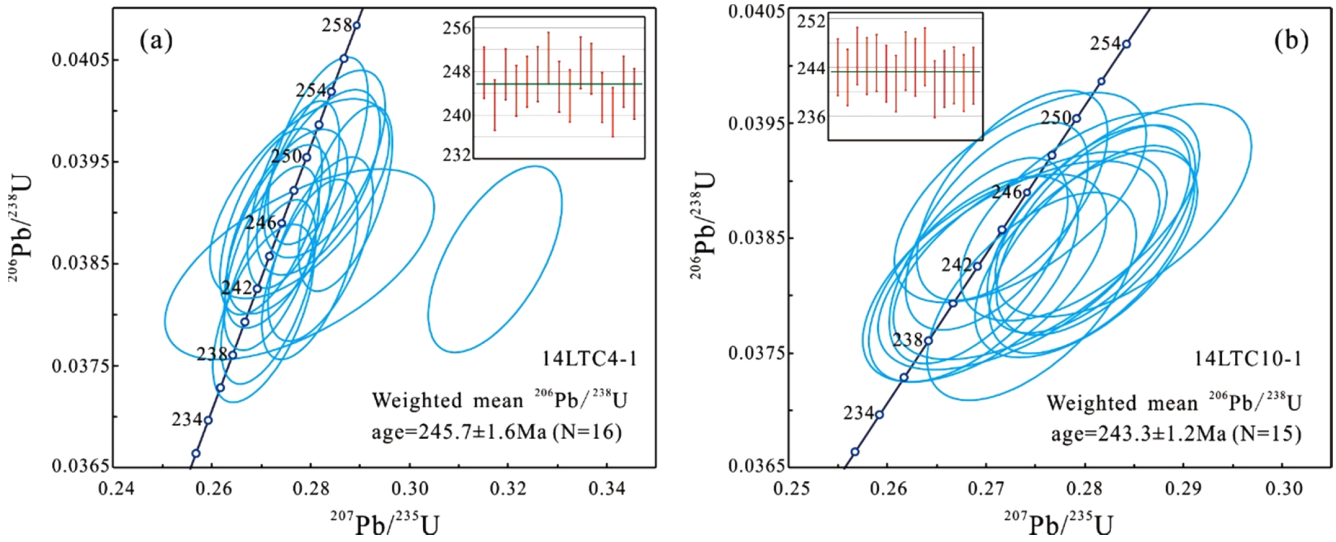

Fig. 5. U-Pb concordia diagrams showing zircon ages obtained by LA-ICP-MS. The insets show weighted average ages.

diorite and monzodiorite, while the intermediate suite was mostly within the fields of monzonite and quartz monzonite.

The mafic samples (SiO_2 = 45.56 to 54.27 wt%) are metaluminous and have high contents of TFe_2O_3 (2.18–9.01 wt%), MgO (6.11–13.84 wt%) and CaO (6.47–10.64 wt%), variable abundances of TiO_2 (0.24–1.05 wt%), Na_2O (1.06–4.29 wt%) and K_2O (0.34–2.88 wt%). In major element Harker plots, most mafic samples defined a continuous evolution trend: Al_2O_3, FeO, MgO, and CaO are negatively correlated with SiO_2, while TiO_2, P_2O_5, MnO, Na_2O, and K_2O are positively correlated.

The intermediate rocks have SiO_2 contents from 57.6 to 63.69 wt% and variable Na_2O (3.87–4.58 wt%), K_2O (3.16–4.08 wt%), MgO (3.33–6.3 wt%) and CaO (3.56–4.61 wt%) contents. However, they show homogeneous TiO_2 (0.69–1.07 wt%) and P_2O_5 (0.25–0.52 wt%). The A/CNK values range from 0.76 to 0.89, showing that the samples are metaluminous and quite different from the coeval Zhuanshanzi and Jianshetun plutons (Liu et al., 2013, 2014).

Applying the classification of Frost et al. (2001), the granitoids mainly belong to the magnesian series (Fig. 6c). In the Na_2O + K_2O-CaO versus SiO_2 diagram, they span the alkali to alkali-calcic fields. As with the mafic rocks, they also defined an evolution trend: TiO_2, Al_2O_3, FeO, P_2O_5, MgO, CaO, MnO, and K_2O are negatively correlated with SiO_2, while Na_2O is weakly positively correlated with SiO_2.

For trace elements, the mafic rocks are characterized by high Cr (up to 849 ppm), Ni (up to 254 ppm) and Sr (up to 1039 ppm), but low Nb (< 9 ppm) and Ta (< 0.7 ppm); they also show high Ba/Nb (52.4–198.1), Ba/Zr (1.9–3.9), Rb/Y (0.6–6.0) and Th/Zr (0.02–0.03), but low Nb/Zr (0.02–0.05) and Nb/Y (0.06–0.5). In contrast, the intermediate rocks are characterized by high Ba (628–972 ppm), Sr (636–881 ppm), Cr (136–440 ppm), Ni (61–164 ppm), Sr/Y (38–71) and La/Yb (13–16), as well as much higher Nb (< 12 ppm) and Ta (< 1.2 ppm).

The intermediate rocks display enrichment in light REEs (LREE)

https://doi.org/10.1007/s12303-020-0004-0

Table 2. Major (wt%) and trace elements (ppm) contents for the Luotuochang complex from Balinzuoqi area, Inner Mongolia

Sample	14LTC1	14LTC2	14LTC3	14LTC4	14LTC5	14LTC6	14LTC7	14LTC8	14LTC9	14LTC10	BL-1	BL-2	BL-3	BL-4
SiO_2	59.88	59.87	59.89	60.86	63.06	63.69	57.60	58.03	52.77	52.39	54.27	49.78	45.56	46.04
TiO_2	0.73	0.77	0.96	0.88	0.72	0.69	1.07	0.99	1.01	1.05	0.97	0.89	0.24	0.25
Al_2O_3	13.99	13.90	15.45	15.15	15.70	15.39	16.00	16.09	15.24	15.11	15.35	16.17	16.27	15.88
Fe_2O_3	1.64	2.03	1.59	1.50	1.45	1.39	1.69	1.71	2.20	2.18	2.20	2.24	3.18	2.98
FeO	3.44	3.14	3.32	3.23	2.57	2.53	3.84	3.55	4.75	5.06	4.88	5.53	5.51	6.03
MnO	0.10	0.09	0.09	0.08	0.07	0.07	0.10	0.08	0.12	0.14	0.16	0.13	0.13	0.14
MgO	6.30	6.25	4.77	4.41	3.41	3.33	4.82	4.77	7.90	8.12	6.11	9.96	13.84	13.29
CaO	4.45	4.51	4.61	4.05	3.70	3.56	4.34	4.54	6.47	6.52	9.27	8.60	10.64	10.48
Na_2O	3.90	3.87	4.52	4.22	4.58	4.50	4.51	4.46	3.94	3.83	4.29	2.72	1.06	1.26
K_2O	3.39	3.44	3.31	3.64	3.16	3.29	4.03	4.08	2.88	2.86	0.48	0.77	0.34	0.38
P_2O_5	0.35	0.37	0.33	0.30	0.26	0.25	0.52	0.50	0.73	0.76	0.22	0.22	0.04	0.03
LOI	1.08	1.37	0.96	0.99	1.14	1.02	0.99	0.69	1.02	1.03	1.54	2.73	2.91	2.99
Total	99.25	99.61	99.80	99.31	99.82	99.71	99.51	99.49	99.03	99.05	99.73	99.74	99.73	99.75
Ba	951	972	761	690	716	687	723	628	573	535	280	198	92.2	92.3
Rb	85.2	86.4	95.4	113	79.6	84.0	151	147	103	100	10.7	25.2	10.5	11.6
Sr	883	884	881	871	698	687	642	636	989	1039	314	665	696	730
Y	12.4	13.2	14.9	14.5	11.0	11.4	16.8	15.8	17.1	17.4	18.1	14.3	8.54	8.34
Zr	213	206	218	201	221	201	505	501	305	237	94.6	57	31.5	23.5
Nb	5.29	5.11	5.88	5.90	5.27	5.61	14.3	11.9	8.41	8.79	5.34	2.53	0.66	0.47
Th	6.50	6.68	6.86	5.88	3.77	8.87	18.3	13.5	8.49	7.40	2.73	1.29	0.66	0.41
Ga	17.1	17.1	18.3	17.8	18.0	17.8	20.9	21.0	19.9	19.2	19.5	16.3	12.7	12.7
Ni	164	155	73.0	61.3	65.9	66.1	108	106	186	197	117	212	254	249
V	125	128	131	121	85.8	85.5	125	117	166	166	168	163	94.8	104
Cr	440	396	190	166	136	141	257	246	519	534	326	652	849	702
Hf	5.55	5.56	5.60	5.08	5.56	5.24	12.6	12.3	7.41	6.03	2.35	1.53	0.97	0.78
Cs	3.39	3.51	6.05	6.98	4.20	4.38	8.43	11.0	8.69	8.87	0.61	1.17	4.51	5.58
Sc	15.0	16.3	16.3	14.7	9.97	10.4	13.6	13.0	18.6	19.5	20.5	27.1	24.0	25.8
Ta	0.49	0.48	0.50	0.47	0.36	0.45	1.12	1.02	0.68	0.67	0.31	0.17	0.05	0.03
Co	23.5	23.4	14.5	16.3	13.5	13.1	18.7	18.7	30.7	32.2	26.1	39.6	56.6	57.1
U	1.63	1.73	3.35	2.13	1.21	1.52	3.52	3.29	3.28	2.94	0.81	0.40	0.23	0.15
La	23.0	25.8	25.1	23.6	22.2	23.9	34.3	32.4	30.2	30.3	16.2	9.40	4.51	3.86
Ce	53.6	58.5	59.3	56.7	50.3	54.6	80.1	77.9	73.3	75.5	33.6	22.6	10.0	8.79
Pr	6.13	6.97	6.92	6.57	5.77	6.22	9.56	8.94	8.73	9.04	4.37	3.17	1.48	1.27
Nd	23.5	26.8	26.1	23.5	20.2	21.6	35.3	31.9	33.0	34.5	19.2	14.9	7.10	6.52
Sm	5.23	5.89	5.97	5.37	4.54	4.78	7.11	6.66	7.01	7.15	3.98	3.15	1.74	1.65
Eu	1.46	1.55	1.76	1.53	1.30	1.32	1.61	1.58	1.77	1.93	1.66	1.08	0.65	0.68
Gd	4.85	5.40	5.63	5.28	4.24	4.55	6.85	6.49	6.83	7.12	3.48	2.94	1.72	1.68
Tb	0.59	0.66	0.72	0.66	0.52	0.57	0.83	0.77	0.82	0.84	0.54	0.44	0.28	0.27
Dy	3.14	3.53	4.00	3.66	2.87	3.10	4.45	4.25	4.48	4.59	3.42	2.76	1.69	1.65
Ho	0.61	0.67	0.77	0.71	0.57	0.59	0.87	0.80	0.85	0.87	0.64	0.52	0.32	0.30
Er	1.61	1.71	2.07	1.92	1.49	1.57	2.31	2.10	2.23	2.26	1.88	1.51	0.89	0.88
Tm	0.24	0.26	0.31	0.29	0.23	0.24	0.35	0.32	0.32	0.33	0.27	0.21	0.12	0.13
Yb	1.58	1.72	1.98	1.88	1.50	1.54	2.32	2.11	1.99	2.05	1.85	1.43	0.84	0.79
Lu	0.24	0.25	0.29	0.28	0.22	0.23	0.34	0.32	0.29	0.29	0.25	0.19	0.11	0.11
ΣREE	125.78	139.71	140.92	131.95	115.95	124.81	186.30	176.54	171.82	176.77	91.34	64.31	31.45	28.56
δEu	0.87	0.83	0.91	0.87	0.89	0.85	0.70	0.73	0.77	0.82	1.33	1.07	1.14	1.23
$(La/Yb)_N$	10.44	10.76	9.09	9.00	10.62	11.13	10.60	11.01	10.89	10.60	6.28	4.72	3.84	3.50

Note: $(La/Yb)_N$ values are La/Yb ratios normalized to chondrite values after Sun and McDonough (1989).

(La_N/Yb_N = 9.00–11.13) with small negative Eu anomalies (Eu/Eu* = 0.70–0.91) (Fig. 7a). Positive K and Sr anomalies with negative Nb, Ta, Nd and Y anomalies were identified when plotted against the primitive mantle-normalized spidergram (Fig. 7b). Sr and

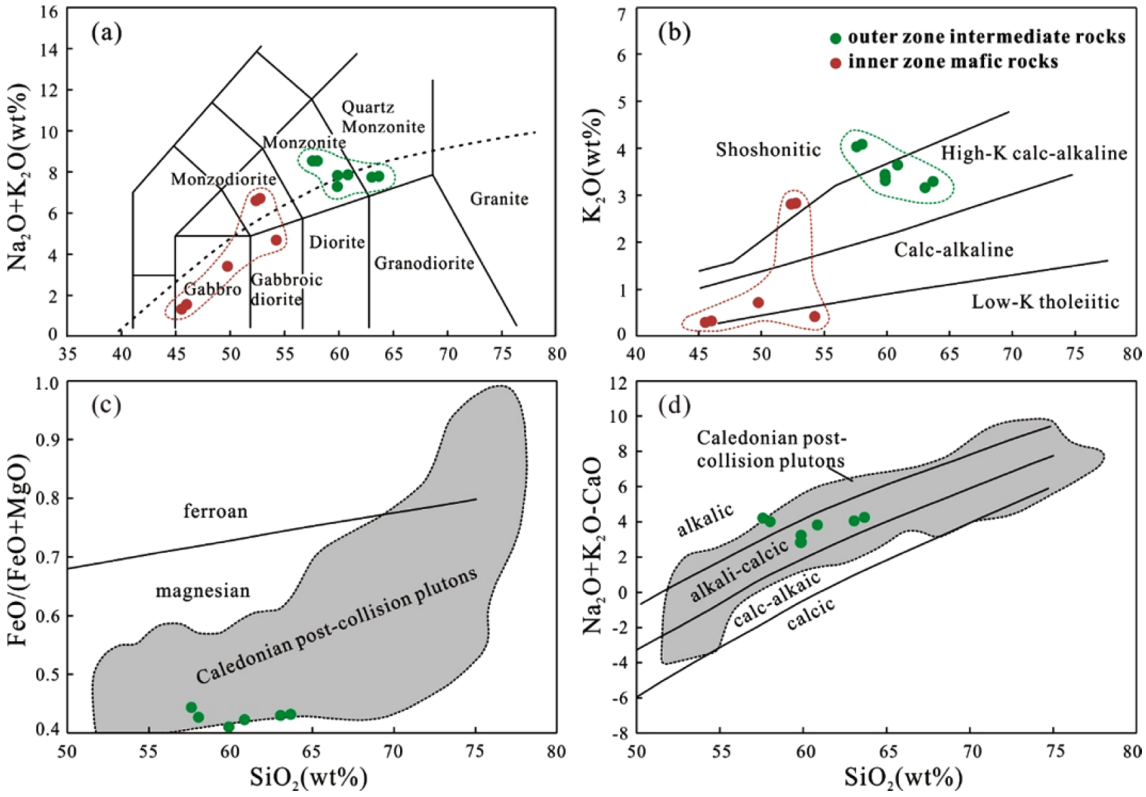

Fig. 6. Classification diagrams for samples from the Luotuochang complex. (a) Total alkalis versus silica (after Le Maitre et al., 2002). (b) K_2O versus SiO_2 (after Rickwood, 1989). (c) FeO/(FeO + MgO) versus SiO_2 (after Frost et al., 2001). (d) Na_2O + K_2O-CaO versus SiO_2 (after Frost et al., 2001).

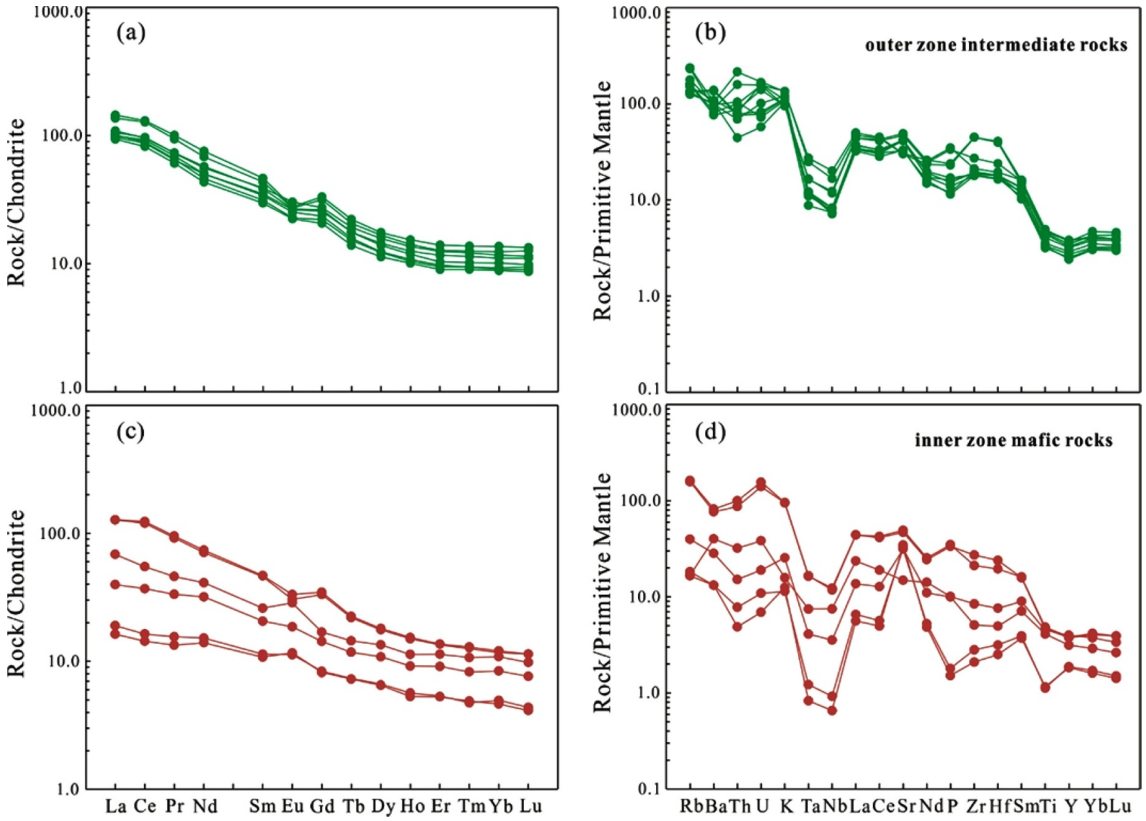

Fig. 7. (a and c) Chondrite-normalized rare earth element patterns and (b and d) primitive mantle-normalized trace element spider diagrams for the Luotuochang complex. The chondrite primitive mantle values are from Sun and McDonough (1989).

https://doi.org/10.1007/s12303-020-0004-0

Table 3. Zircon Hf isotopic compositions of the Luotuochang complex from Balinzuoqi area, Inner Mongolia

Spot No.	Age (Ma)	$^{176}Yb/^{177}Hf$	$^{176}Lu/^{177}Hf$	$^{176}Hf/^{177}Hf$	2σ	εHf(0)	εHf(*t*)	T_{DM}(Ma)	T_{DM}^{C}(Ma)	$f_{Lu/Hf}$
14LTC4-1 Monzonite										
1	248	0.0675	0.0022	0.282988	0.000022	7.6	12.7	387	462	−0.93
2	242	0.0259	0.0008	0.283005	0.000028	8.2	13.4	348	412	−0.98
3	247	0.0616	0.0020	0.282926	0.000021	5.4	10.5	475	600	−0.94
4	244	0.0531	0.0017	0.282923	0.000021	5.3	10.4	476	606	−0.95
5	246	0.0309	0.0011	0.283006	0.000023	8.3	13.5	350	410	−0.97
6	247	0.0258	0.0009	0.282859	0.000023	3.1	8.4	556	740	−0.97
7	250	0.0317	0.0011	0.282976	0.000027	7.2	12.5	392	476	−0.97
8	245	0.0448	0.0015	0.282870	0.000024	3.5	8.6	549	723	−0.95
9	244	0.0442	0.0015	0.282980	0.000022	7.4	12.5	391	475	−0.95
10	250	0.0209	0.0007	0.282949	0.000019	6.3	11.6	426	533	−0.98
11	248	0.0328	0.0011	0.282951	0.000022	6.3	11.6	428	534	−0.97
12	243	0.0374	0.0013	0.282934	0.000024	5.7	10.9	455	577	−0.96
13	244	0.0514	0.0016	0.282917	0.000023	5.1	10.2	483	618	−0.95
14	241	0.0368	0.0012	0.282996	0.000025	7.9	13.0	365	437	−0.96
15	246	0.0262	0.0008	0.282901	0.000020	4.6	9.8	495	645	−0.98
16	244	0.0386	0.0013	0.282976	0.000029	7.2	12.4	395	482	−0.96
14LTC10-1 Gabbro										
1	244	0.0235	0.0008	0.282941	0.000020	6.0	11.2	439	556	−0.98
2	242	0.0262	0.0009	0.282923	0.000017	5.3	10.5	466	599	−0.97
3	246	0.0210	0.0007	0.282944	0.000019	6.1	11.4	433	547	−0.98
4	244	0.0234	0.0008	0.282959	0.000018	6.6	11.8	413	515	−0.98
5	245	0.0226	0.0008	0.282936	0.000017	5.8	11.1	446	566	−0.98
6	243	0.0093	0.0003	0.282932	0.000017	5.7	10.9	446	572	−0.99
7	241	0.0151	0.0005	0.282967	0.000016	6.9	12.1	399	496	−0.98
8	245	0.0148	0.0005	0.282945	0.000021	6.1	11.4	430	543	−0.98
9	244	0.0286	0.0010	0.282880	0.000020	3.8	9.0	528	696	−0.97
10	246	0.0228	0.0008	0.282900	0.000018	4.5	9.8	497	647	−0.98
11	240	0.0239	0.0009	0.282953	0.000017	6.4	11.5	423	532	−0.97
12	242	0.0118	0.0004	0.282887	0.000022	4.1	9.3	510	675	−0.99
13	243	0.0159	0.0006	0.282924	0.000020	5.4	10.6	460	593	−0.98
14	241	0.0258	0.0009	0.282820	0.000023	1.7	6.8	611	832	−0.97
15	243	0.0202	0.0007	0.282942	0.000022	6.0	11.2	436	553	−0.98

Ba are high in most of the intermediate rocks. The mafic rocks show variable LREE enrichment patterns (La_N/Yb_N = 3.50–10.89) with small negative or positive Eu anomalies (Eu/Eu* = 0.77–1.33) (Fig. 7c).

5.3. Lu-Hf Isotope Composition

Lu-Hf isotopic data of zircons from the intermediate (14LTC4-1) and mafic (14LCT10-1) rock samples are given in Table 3. Variations in Hf isotope ratios ($\varepsilon_{Hf}(t)$) with their U-Pb ages (*t*) are plotted in Figure 8a. Zircon Hf analyses were undertaken on the same grains as those used for U-Pb dating (Fig. 4).

Sixteen Lu-Hf analyses were obtained from 16 dated zircon grains from the granitoid sample (14LCT4-1). $^{176}Hf/^{177}Hf$ ranges from 0.282859 to 0.283006. The calculated $\varepsilon_{Hf}(t)$ range from +8.4 to +13.5, and the Hf model ages (T_{DM}) range from 348 to 556 Ma. Fifteen zircon grains from the mafic rock sample (14LTC10-1) were also analyzed and had $^{176}Hf/^{177}Hf$ of 0.282820 to 0.282967, corresponding to $\varepsilon_{Hf}(t)$ of +6.8 to +12.1 and T_{DM} ages of 399 to 611 Ma.

5.4. Whole-rock Sr-Nd Isotope Composition

Whole-rock Rb-Sr and Sm-Nd isotopic compositions of seven samples are presented in Table 4 and Figure 8b. The initial $^{87}Sr/^{86}Sr$ (I_{Sr}) and $\varepsilon_{Nd}(t)$ values were calculated using the new zircon U-Pb ages for the outer zone granitoids and inner zone mafic rocks. All of these samples exhibit similar Sr-Nd isotopic compositions

Table 4. Sr-Nd isotopic compositions for the Luotuochang complex from Balinzuoqi area, Inner Mongolia

Sample no.	Age (Ma)	Rb (ppm)	Sr (ppm)	$^{87}Rb/^{86}Sr$	$^{87}Sr/^{86}Sr$	2σ	I_{Sr}	Sm (ppm)	Nd (ppm)	$^{147}Sm/^{144}Nd$	$^{143}Nd/^{144}Nd$	2σ	$\varepsilon_{Nd}(0)$	$\varepsilon_{Nd}(t)$	T_{DM} (Ma)	T_{2DM} (Ma)	$f_{Sm/Nd}$
14LCT1	246	85.2	883	0.2792	0.70499	0.000011	0.70401	5.32	23.5	0.1369	0.512653	0.000009	0.3	2.2	990	843	−0.30
14LCT2	246	86.4	884	0.2828	0.70495	0.000017	0.70396	5.89	26.8	0.1329	0.512671	0.000010	0.6	2.6	907	804	−0.32
14LCT5	246	79.6	698	0.3300	0.70493	0.000016	0.70378	4.54	20.2	0.1359	0.512746	0.000009	2.1	4.0	795	692	−0.31
14LCT6	246	84.0	687	0.3538	0.70502	0.000012	0.70378	4.78	21.6	0.1338	0.512702	0.000013	1.2	3.2	858	757	−0.32
14LCT7	243	151	642	0.6806	0.70636	0.000013	0.70401	7.11	35.3	0.1218	0.512766	0.000011	2.5	4.8	640	624	−0.38
14LCT8	243	147	636	0.6688	0.70623	0.000013	0.70392	6.66	31.9	0.1263	0.512637	0.000012	0.0	2.2	898	841	−0.36
14LCT9	243	103	989	0.3014	0.70483	0.000014	0.70379	7.01	33.0	0.1285	0.512654	0.000011	0.3	2.4	890	819	−0.35

Note: $\varepsilon_{Nd} = [(^{143}Nd/^{144}Nd)_{sample}/(^{143}Nd/^{144}Nd)_{CHUR} - 1] \times 10{,}000$, $f_{sm/Nd} = (^{147}Sm/^{144}Nd)_{sample}/(^{147}Sm/^{144}Nd)_{CHUR} - 1$, where $(^{147}Sm/^{144}Nd)_{CHUR} = 0.1967$, $(^{143}Nd/^{144}Nd)_{CHUR} = 0.512638$.

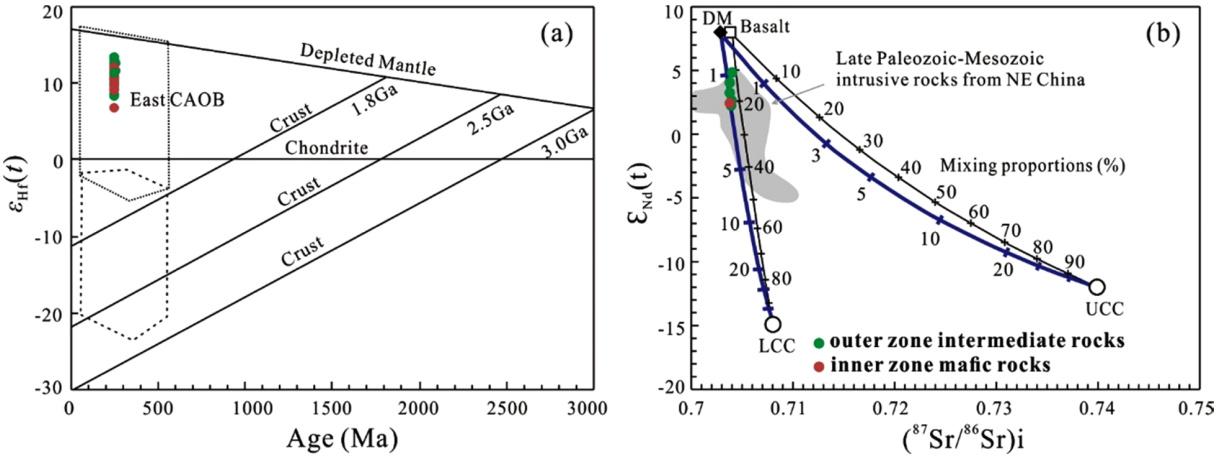

Fig. 8. Plots of (a) $\varepsilon_{Hf}(t)$ versus U-Pb age of zircons and (b) $\varepsilon_{Nd}(t)$ versus $(^{87}Sr/^{86}Sr)i$ for the Luotuochang complex. The numbers indicate the percentages of participation of the crustal materials. The field for late Paleozoic–Mesozoic intrusive rocks in NE China is from Wu et al. (2003, 2004). For detailed calculation parameters of Nd, $\varepsilon_{Nd}(t)$, Sr and $(^{87}Sr/^{86}Sr)i$ refer to Wu et al. (2003).

and record moderate I_{Sr} values (0.70483–0.70636) and weak positive $\varepsilon_{Nd}(t)$ values (+2.2 to +4.8), with Neoproterozoic Nd model ages of 0.64–0.99 Ga, similar to the Paleozoic and Mesozoic granitoids in the CAOB.

6. DISCUSSION

6.1. Early Triassic Magmatism along the Solonker Suture Zone

The Luotuochang complex was previously categorized as Late Triassic in age using Rb-Sr isotopic ages and a lithostratigraphic interpretation (Xu, 1986). Our new zircon data indicate that it is an Early Triassic complex ($^{206}Pb/^{238}U$ ages of 243–246 Ma).

In the past few years, several Early Triassic magmatic rocks have been studied from the Linxi and Balinzuoqi areas (Li et al., 2007; Liu et al., 2007; Zhang et al., 2008; Wu et al., 2011; Liu et al., 2013, 2014) (Fig. 1). These include the Zhuanshanzi (246 Ma) and Jianshetun (249 Ma) granodiorites (Liu et al., 2013, 2014), Shuangjing granite (237 Ma, Li et al., 2007), Xinlin granodiorite (241 Ma, Wu et al., 2011) and some volcanic rocks in the Lindong area (243–252 Ma, Zhang et al., 2008). Detrital zircons from Early–Middle Triassic sandstones in the area also displayed a dominant age population of 214–251 Ma, which possibly derived from Early Triassic magmatic rocks along the Solonker suture zone (Zhu et al., 2017). These magmatic rocks constitute a magmatic belt sub-parallel with the Solonker–Xar Moron suture zone (Fig. 1). The Early Triassic magmatic rocks have geochemical features akin to adakite-like rocks and are probably related to fossil slab break-off during crustal compression and thickening soon after the final closure of the Paleo-Asia Ocean (Liu et al., 2012; Li et al., 2014). Therefore, constraining the origin and tectonic setting of the Triassic magmatic rocks is helpful in understanding the late tectonic stage of the PAO tectonic domain.

6.2. Petrogenesis

The geochemical composition and field observations of the intermediate and mafic rocks exclude the possibility that these magma bodies were generated separately and one intruded into

https://doi.org/10.1007/s12303-020-0004-0

the other accidentally. With their hornblende-dominated mafic minerals, elevated alkali values, Ba-Sr abundances and some other typical geochemical characteristics, the Luotuochang complex bears a remarkable resemblance to the so-called 'appinite suite' from late Caledonian and late Variscan granitoid batholiths in Europe. This suite includes several types of mafic to intermediate rocks characterized by hydrous mineral assemblages with hornblende and biotite and by an overall andesitic to basaltic composition of calc-alkaline affinity (Fowler and Henney, 1996; Pitcher, 1997; Fowler et al., 2001; Zhang et al., 2012a, 2012b).

After its description from the Appin district of Scotland (Bailey and Maufe, 1916), the appinite suite has been widely documented from various calc-alkaline granitoid batholiths worldwide (Zhang et al., 2012a, 2012b; Zhong et al., 2014; Xiong et al., 2015). In terms of origin and tectonic setting, the appinite suite is unique in that (1) it commonly forms the mafic precursors of granitoid batholiths and thus can support mantle involvement in granite genesis (Fowler and Henney, 1996; Pitcher, 1997; Bea et al., 1999; Fowler et al., 2001, 2008; Atherton and Ghani, 2002; Castro et al., 2003), and (2) it has the general characteristics of the final orogeny stage and can even be indicative of critical post-subduction events, such as slab break-off or delamination (Atherton and Ghani, 2002; Kovalenko et al., 2005; Ye et al., 2008).

6.2.1. Petrogenesis of the mafic rocks

The mafic rocks are characterized by high MgO (up to 13.84 by weight), Cr (up to 849 ppm), Ni (up to 254 ppm), Sr (up to 1039 ppm) and Mg# (63–88) values, implying a mantle source for the magma without crustal contamination (Wilson, 1989; Patino and Beard, 1995; Patino and McCarthy, 1997). Mafic magma is generally derived from two mantle sources: partial melting of asthenospheric mantle and metasomatization of lithospheric mantle (McDonough, 1990; Mckenzie and O'Nions, 1995). The mafic magmas from asthenospheric mantle usually have higher TiO_2 (e.g., average TiO_2 in ocean island basalt (OIB) is 2.86%), whereas magmas from the lithospheric mantle have relatively lower TiO_2 (Lightfoot et al., 1993; Ewart et al., 1998). The TiO_2 contents of the Luotuochang mafic rocks are much lower than OIB, implying that they have a lithospheric mantle source. The relatively higher La/Nb (3.0–8.3; i.e., > 1.5) and La/Ta (44.4–113.5; i.e., > 30) compared to mafic rocks derived from asthenospheric mantle also suggest that they were sourced from lithospheric mantle (Thompson and Morrison, 1988; Saunder et al., 1991).

However, the REE patterns of the mafic rocks show enrichment in LREEs relative to heavy REEs (HREEs) and their mantle-normalized profiles display negative Ta, Nb and Ti anomalies, showing a subducted material imprint on the rock source. Moreover, high Ba/Nb (52.4–198.1), Ba/Zr (1.9–3.9), Rb/Y (0.6–6.0) and Th/Zr (0.02–0.03), but low Nb/Zr (0.02–0.05) and Nb/Y (0.06–0.5) (Figs. 9a and b) indicate that the mantle source was previously enriched in slab-derived fluid rather than hydrous melt (Turner et al., 1996; Kepezhinskas et al., 1997).

Published geochemical studies have demonstrated that the mantle component beneath Inner Mongolia has gone through a strong metasomatism process due to PAO subduction (Liu et al., 2012; Pan et al., 2013; Zou et al., 2014). Geochemical and isotopic features of the Triassic high-Mg andesites from the Linxi area suggest that it could be derived from a subducted Paleo-Asian oceanic slab with sediments shed from the NCC. Accordingly, the metasomatized lithospheric mantle might serve as the primitive magma source for the Luotuochang mafic rocks.

6.2.2. Petrogenesis of the intermediate rocks

The appinite suite generally forms the mafic precursor of granitoid batholiths and thus suggests mantle involvement in granite genesis (Bea et al., 1999; Atherton and Ghani, 2002; Castro et al., 2003; Ye et al., 2008; Zhang et al., 2012a). However, the felsic end-members in the appinitie-granite suite commonly have a high Ba-Sr (Fowler and Henney, 1996; Ye et al., 2008; Zhang et al., 2012) or high Sr/Y adakitic geochemical affinity (Moyen, 2009). High Ba-Sr granitoids are characterized by alkali-rich, high K_2O and K_2O/Na_2O, high Ba, Sr and LREEs, and low Nb, Ta and HREEs, which are distinct from typical I-, S- and A-type granitoids (Tarney and Jones, 1994; Fowler et al., 2001, 2008; Pan et al., 2016).

Intermediate rocks from the Luotuochang complex are enriched in K_2O (3.16–4.08 wt% with K_2O/Na_2O of 0.69–0.91) and characterized by high Ba (628–972 ppm) and Sr (636–881 ppm) contents, comparable to typical high Ba-Sr granitoids (Fig. 9c). Petrogenesis of high Ba-Sr granitoids has been extensively studied, but no consensus has been reached, and a variety of petrogenetic models have been proposed, including: (1) partial melting of subducted ocean plateaus (Tarney and Jones, 1994); (2) partial melting of mafic lower crust (Ye et al., 2008; Choi et al., 2009); (3) partial melting of enriched lithospheric mantle metasomatized by asthenosphere-derived carbonatitic melts or subduction-related fluids and/or melts (Eklund et al., 1998; Fowler et al., 2001, 2008; Peng et al., 2013).

The intermediate rocks from the Luotuochang complex have low initial $^{87}Sr/^{86}Sr$ (0.70483 to 0.70636), high $\varepsilon_{Nd}(t)$ values (+2.2 to +4.8), variable $(^{143}Nd/^{144}Nd)_i$ (0.512637 to 0.512766) and young T_{DM2} (Nd) ages (843 to 624 Ma), implying a mantle or juvenile lower crustal source. In addition, these samples have transitional Nb/Ta (10.7 to 14.6) between mantle and global lower crust and are close to the primitive mantle (McDonough and Sun, 1995). Furthermore, the Cr (136–440 ppm) and Ni (61–164 ppm) contents of these samples are high, which implies that the magma of these rocks was mainly derived from the mantle with possible juvenile lower crust involvement.

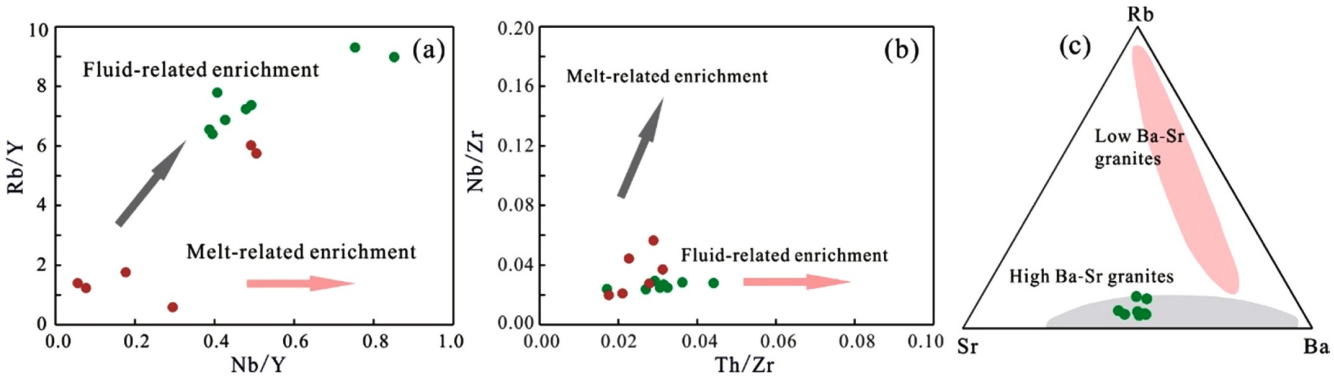

Fig. 9. (a) Rb/Y versus Nb/Y, (b) Nb/Zr versus Th/Zr and (c) Sr-Rb-Ba plots for the Luotuochang complex (modified after Tarney and Jones, 1994).

A simple mixing model was employed to estimate the proportions of mantle-to-crust components using Sr-Nd isotopic data (Fig. 8b). The data show that upper crust components (UCC) had little or no role in the generation of the studied intermediate rocks, whereas mantle-derived basaltic magma and the lower crust (LCC) are the two major components. This does not unequivocally mean that the intermediate rocks were formed by mixing mantle-derived magma and lower crustal melts in such proportions. Rather, it suggests that the magmas were produced by melting a mixed lithology containing a lower crustal gneiss intruded or underplated by a mantle-derived magma (Wu et al., 2003; Liu et al., 2010).

6.3. Tectonic Implications

Although many studies have been carried out in southeastern Inner Mongolia, the timing of the final closure of the PAO is still controversial. Two final closure sequences and ages have been proposed: (1) late Devonian to early Carboniferous, followed by widespread post-orogenic extension and rifting during the late Carboniferous–Permian (Tang, 1990; Shao et al., 2014, 2015; Tong et al., 2015; Xu et al., 2015; Zhao et al., 2016); (2) latest Permian to Early Triassic, when the PAO slab underwent continuous subduction and accretion over a prolonged period of time until the collision of the Siberian craton and NCC in the latest Permian or Early–Middle Triassic (Wang and Liu, 1986; Chen et al., 2000, 2009; Xiao et al., 2003, 2009, 2015; Jian et al., 2008, 2010). Overall, these conflicting viewpoints reflect uncertainties in the tectonic setting from the late Paleozoic to early Mesozoic of southeastern Inner Mongolia.

The Triassic Luotuochang complex contains hornblende-dominated mafic minerals, elevated alkali and Ba-Sr abundances and some other typical geochemical characteristics that suggest it is an appinite complex. Such rocks are generally considered emplaced during the final stage of orogeny and linked to critical post-subduction events, such as slab break-off or delamination (Atherton and Ghani, 2002; Kovalenko et al., 2005; Ye et al., 2008; Zhang et al., 2012a, 2012b). The mafic rocks of this complex have high contents of MgO, Cr, Ni and Sr, lower contents of TiO_2 and higher La/Nb and La/Ta ratios. These features, combined with their $\varepsilon_{Hf}(t)$ and $\varepsilon_{Nd}(t)$ values, suggest that they have imprinted on subducted material and probably resulted from partial melting of the metasomatized lithospheric mantle. The geochemical compositions of intermediate rocks indicate that they belong to high Ba-Sr granitoids and were generated by magma mixing that involved different proportions of mantle- and crust-derived materials. The magma-mixing processes most likely occurred in a subduction or post-orogenic tectonic setting (Blundy and Sparks, 1992; Sylvester, 1998; Tepley et al., 2000; Annen et al., 2006; Reubi and Blundy, 2009).

This study and the available geological data are most supportive of a post-orogenic tectonic setting in southeastern Inner Mongolia during the early Mesozoic. This interpretation is supported by additional evidence. Previous work has described a late Carboniferous to early Permian extensional event that resulted in a series of late Carboniferous to early Permian post-orogenic alkaline magmatic rocks and bimodal volcanic rocks in the eastern and central areas of Inner Mongolia (Zhang et al., 2008, 2017). Two huge early–middle Permian peralkaline-alkaline rock belts have been documented from the north to the south in the eastern segment of the CAOB, the Erenhot–Dongwuqi Belt and the northern margin of the NCC (Hong et al., 1994; Tong et al., 2015; Zhao et al., 2016a). The emplacement of these magmatic rocks was commonly considered an extensional setting. Furthermore, there are a large number of contemporaneous granitoids and bimodal volcanic rocks between these two belts, such as the Xilinhot A-type granite, the Qianjinchang pluton and the Xiwuqi bimodal volcanic rocks (Shi et al., 2004; Zhang et al., 2008; Wang et al., 2018). Second, the stratigraphy and sedimentary environment of the Carboniferous–Permian in NE China shows a large ENE-NE-trending littoral-neritic to continental sedimentary basin, starting in the west from Ejinqi and extending eastwards through southeastern Inner Mongolia into Jilin and Heilongjiang provinces. The late Carboniferous–

https://doi.org/10.1007/s12303-020-0004-0

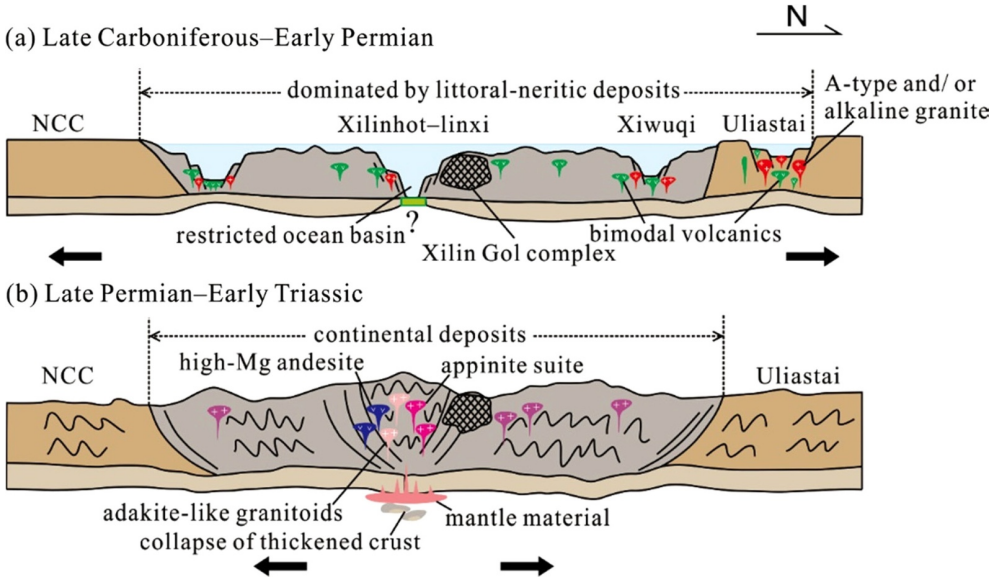

Fig. 10. Cartoon showing the late tectonic evolution of the PAO. (a) The late Carboniferous–early Permian post-orogenic extensional event resulted in a series of alkaline granitoids and bimodal volcanic rocks generated. (b) Following the PAO closure, a collisional orogeny occurred in the late Permian to Early Triassic, accompanied by intense orogenic uplift, crustal thickening and magmatism.

middle Permian is dominated by littoral-neritic deposits and the late Permian is mainly continental deposits. They unconformably overlie Precambrian basement, ophiolitic mélanges and early Paleozoic magmatic arcs (Zhao et al., 2016b, 2017; Zhu et al., 2017). Third, the Early Triassic magmatic belt that is sub-parallel to the Solonker suture zone has geochemical features akin to adakite-like rocks and was probably generated in an extensional environment (Li et al., 2013; Liu et al., 2013, 2014). Finally, it was confirmed that the Erenhot-Hegenshan, Xiwuqi-Zhunmubutai, and Solonker-Linxi ophiolite belts were formed in a newly opened ocean basin rather than the remnants of the PAO (Luo et al., 2016; Yang et al., 2017; Wang et al., 2019).

Thus, we propose a two-stage development model (Fig. 10): (1) the main part of the PAO was closed in southeastern Inner Mongolia prior to the late Carboniferous. A large amount of high potassium calc-alkaline granitoids and bimodal volcanic rocks generated in these areas at 320–275 Ma might be related to the post-orogenic geologic setting; (2) with ongoing extension, a restricted ocean basin could have been formed in southeastern Inner Mongolia and did not close until the early late Permian. The Solonker suture zone represents the termination of this restricted remnant ocean basin. This speculation is corroborated by a study of metamorphic rocks from southeastern Inner Mongolia, which suggests the Solonker suture zone is distinct from typical convergent plate tectonic settings, such as the Pacific and Himalayan-type orogens (Zhang et al., 2016). Following this closure, a collisional orogeny along the Xar Moron River area occurred in the late Permian to Early Triassic, accompanied by intense orogenic uplift, crustal thickening, magmatism and regional metamorphism (Li et al., 2013).

The composition of Luotuochang complex is similar to other known intrusive rocks along the northern NCC, such as the Siziwangqi, Tiejianggeleng and Shichang plutons, all of which were generated in a post-orogenic extensional setting following a crustal thickening event (Zhang et al., 2012b). Their formation was likely the result of lithospheric delamination, upwelling of new mantle material and partial melting of the overlying lower crust after the closure of the PAO. This mechanism can also explain magmatic activities during the post-orogeny in this area.

7. CONCLUSIONS

Our field and laboratory data and their integration with the regional geology lead us to the following conclusions:

(1) LA-ICP-MS zircon U-Pb dating constrains an emplacement age of approximately 243–246 Ma (Triassic) for the Luotuochang appinitic complex near the Solonker suture zone in southeastern Inner Mongolia.

(2) Geochemical and isotopic tracing demonstrates that the mafic rocks derive from metasomatized lithospheric mantle, while the magma of intermediate rocks was mainly derive from the mantle with possible juvenile lower crust involvement.

(3) The formation of this hornblende-rich complex was probably a result of lithospheric delamination, upwelling of new mantle material and partial melting of the overlying lower crust in a post-orogenic setting after the closure of the PAO.

ACKNOWLEDGMENTS

This work was financially supported by the National Natural Science Foundation of China (Grant Number 41802243) and the China Geological Survey Program (Grant Number DD20190358). We gratefully extend our appreciation to professors Sun Lixin, Yang Tiannan and Li Shan, who provided much help and advice during the field work. We are also grateful to anonymous reviewers for their constructive comments.

REFERENCES

Andersen, T., 2002, Correction of common lead in U-Pb analyses that do not report ^{204}Pb. Chemical Geology, 192, 59–79.

Atherton, M.P. and Ghani, A.A., 2002, Slab breakoff: a model for Caledonian, Late Granite syn-collisional magmatism in the orthotectonic (metamorphic) zone of Scotland and Donegal, Ireland. Lithos, 62, 65–85.

Blichert-Toft, J. and Albarède, F., 1997, The Lu-Hf geochemistry of chondrites and the evolution of the mantle-crust system. Earth and Planetary Science Letters, 148, 243–258.

Castro, A., Corretge, L.G., De La, Rosa, J.D., Fernández, C., López, S., Garcia-Moreno, O., and Chacon, H., 2003, The appinite-migmatite complex of Sanabria, NW Iberian Massif, Spain. Journal of Petrology, 44, 1309–1344.

Chen, B., Jahn, B.M., and Tian, W., 2009, Evolution of the Solonker suture zone: constraints from zircon U-Pb ages, Hf isotopic ratios and whole-rock Nd-Sr isotope compositions of subduction- and collision-related magmas and fore-arc sediments. Journal of Asian Earth Sciences, 34, 245–257.

Chen, B., Jahn, B.M., Wilde, S.A., and Xu, B., 2000, Two contrasting Paleozoic magmatic belts in northern Inner Mongolia, China: petrogenesis and tectonic implications. Tectonophysics, 328, 157–182.

Chen, C., Zhang, Z.C., Guo, Z.J., Li, J.F., Feng, Z.S., and Tang, W.H., 2012, Geochronology, geochemistry, and its geological significance of the Permian Mandula mafic rocks in Damaoqi, Inner Mongolia. Science China Earth Sciences, 55, 39–52.

Chen, C., Zhang, Z.C., Li, K., Chen, Y., Tang, W.H., and Li, J.F., 2015, Geochronology, geochemistry, and its geological significance of the Damaoqi Permian volcanic sequences on the northern margin of the North China Block. Journal of Asian Earth Sciences, 97, 307–319.

Fowler, M.B., 1988, Ach'uaine hybrid appinite pipes: evidence for mantle-derived shoshonitic parent magmas in Caledonian granite genesis. Geology, 16, 1026–1030.

Fowler, M.B., Henney, P.J., Darbyshire D.P.F., and Greenwood, P.B., 2001, Petrogenesis of high Ba-Sr granites: the Rogart pluton, Sutherland. Journal of the Geological Society, 158, 521–534.

Frost, B.R., Barnes, C.G., Collins, W.J., Arculus, R.J., Ellis, D.J., and Frost, C.D., 2001, A geochemical classification for granitic rocks. Journal of Petrology, 42, 2033–2048.

Geng, J.Z., Li, H.K., Zhang, J., Zhou, H.Y., and Li, H.M., 2011, Zircon Hf isotope analysis by means of LA-MC-ICP-MS. Geological Bulletin of China, 30, 1508–1513. (in Chinese with English abstract)

Griffin, W.L., Pearson, N.J., Belousova, E., Jackson, S.E., van Achtenberg, E., O'Reilly, S.Y., and Shee, S.R., 2000, The Hf isotopes composition of carbonic mantle: LA-MC-ICP-MS analysis of zircon megacrysts in kimberlites. Geochimica et Cosmochimica Acta, 64, 133–147.

Hong, D.W., Chang, W.J., Huang, H.Z., Xiao, Y.J., Xu, H.M., and Jin, M.Y., 1994, The Permian alkaline granites in central Inner Mongolia and their geodynamic significance. Journal of Southeast Asian Earth Sciences, 10, 169–176.

Jahn, B.M., Windley, B., Natal'in, B., and Dobretsov, N., 2004, Phanerozoic continental growth in Central Asia. Journal of Asian Earth Sciences, 23, 599–603.

Jian, P., Liu, D.Y., Kröner, A., Windley, B.F., Shi, Y.R., Zhang, W., Zhang, F.Q., Miao, L.C., Zhang, L.Q., and Tomurhuu, D., 2010, Evolution of a Permian introceanic arc-trench system in the Solonker suture zone, Central Asian Orogenic Belt, China and Mongolia. Lithos, 118, 169–190.

Jian, P., Liu, D.Y., Kröner, A., Windley, B.F., Shi, Y.R., Zhang, F.Q., Shi, G.H., Miao, L.C., Zhang, W., Zhang, Q., Zhang, L.Q., and Ren, J.S., 2008, Time scale of an early to mid-Paleozoic orogenic cycle of the long-lived Central Asian Orogenic Belt, Inner Mongolia of China: implications for continental growth. Lithos, 101, 233–259.

Khain, E.V., Bibikova, E.V., Kröner, A., Zhuravlev, D.Z., Sklyarov, E.V., Fedotova, A.A., and Kravcheko-Berezhnoy, I.R., 2002, The most ancient ophiolite of the Central Asian fold belt: U-Pb and Pb-Pb zircon ages for the Dunzhugur Complex, Eastern Sayan, Siberia, and geodynamic implications. Earth and Planetary Science Letters, 199, 311–325.

Le Maitre, R.W., Streckeisen, A., Zanettin, B., Le Bas, M.J., Bonin, B., Bateman, P., Bellieni, G., Dudek, A., Efremova, S., Keller, J., Lameyre, J., Sabine, P.A., Schmid, R., Sørensen, H., and Wooley, A.R., 2002, Igneous Rocks: A Classification and Glossary of Terms. Cambridge University Press, Cambridge, 254 p.

Li, J.Y., 2006, Permian geodynamic setting of northeast China and adjacent regions: closure of the Paleo-Asian Ocean and subduction of the Paleo-Pacific Plate. Journal of Asian Earth Sciences, 26, 207–224.

Li, K., Zhang, Z.C., Feng, Z.S., Li, J.F., and Tang, W.H., 2015, Two-phase magmatic events during Late Paleozoic in the north of the central Inner Mongolia–Da Hinggan orogenic belt and its tectonic significance. Acta Geologica Sinica, 89, 272–288. (in Chinese with English abstract)

Li, S., Wang, T., Wilde, S.A., and Tong Y., 2013, Evolution, source and tectonic significance of early Mesozoic granitoid magmatism in the Central Asian Orogenic Belt (central segment). Earth-Science Reviews, 126, 206–234.

Li, S., Wilde, S.A., Wang, T., Xiao, W.J., and Guo, Q.Q., 2016, Latest early Permian granitic magmatism in southern Inner Mongolia, China: implications for the tectonic evolution of the southeastern Central Asian Orogenic Belt. Gondwana Research, 29, 168–180.

Liang, Q. and Grégoire, D.C., 2000, Determination of trace elements in twenty-six Chinese geochemistry reference materials by inductively coupled plasma-mass spectrometry. Geostandards & Geoanalytical Research, 24, 51–63.

Liang, R.X., 1994, The features of ophiolites in the central sector of Inner Mongolia and its geological significance. Regional Geology of China, 1, 37–45. (in Chinese with English abstract)

 https://doi.org/10.1007/s12303-020-0004-0

Liu, J.F., Chi, X.G., Zhao, Z., Hu, Z.C., and Chen, J.Q., 2013, Zircon U-Pb age and petrogenetic discussion on Jianshetun adakite in Balinyouqi, Inner Mongolia. Acta Petrologica Sinica, 29, 827–839. (in Chinese with English abstract)

Liu, J.F., Li, J.Y., Chi, X.G., Qu, J.F., Hu, Z.C., and Guo, C.L., 2014, Petrological and geochemical characteristics of the Early Triassic granite belt in southeastern Inner Mongolia and its tectonic setting. Acta Geologica Sinica, 88, 1677–1690. (in Chinese with English abstract)

Liu, Y.S., Hu, Z.C., Gao, S., Günther, D., Xu, J., Gao, C.G., and Chen, H.H., 2008, In situ analysis of major and trace elements of anhydrous minerals by LA-ICP-MS without applying an internal standard. Chemical Geology, 257, 34–43.

Liu, Y.S., Wang, X.H., Wang, D.B., He, D.T., Zong, K.Q., Gao, C.G., Hu, Z.C., and Gong, H.J., 2012, Triassic high-Mg adakitic andesites from Linxi, Inner Mongolia: insights into the fate of the Paleo-Asian ocean crust and fossil slab-derived melt-peridotite interaction. Chemical Geology, 328, 89–108.

Ludwig, K.R., 2003, Isoplot 3.00: a geochronological toolkit for Microsoft Excel. Special Publication No. 4. Berkeley Geochronology Center, Berkeley, 70 p.

Luo, Z.W., Xu, B., Shi, G.Z., Zhao, P., Faure, M., and Chen, Y., 2016, Solonker ophiolite in Inner Mongolia, China: a late Permian continental margin-type ophiolite. Lithos, 261, 72–91.

McDonough, W.F., 1990, Constraints on the composition of the continental lithospheric mantle. Earth and Planetary Science Letters, 101, 1–18.

McKenzie, D. and O'Nions, R.L., 1995, The source regions of oceanic island basalts. Journal of Petrology, 36, 133–159.

Miao, L., Zhang, F., Fan, W.M., and Liu, D., 2007, Phanerozoic evolution of the Inner Mongolia–Daxinganling orogenic belt in North China: constraints from geochronology of ophiolites and associated formations. In: Zhai, M.G., Windley, B.F., Kusky, T.M., and Meng, Q.R. (eds.), Mesozoic Sub-continental Lithospheric Thinning Under Eastern Asia. Geological Society, London, Special Publications, 280, p. 223–237. https://doi.org/10.1144/SP280.11

Miao, L.C., Fan, W.M., Liu, D.Y., Zhang, F.Q., Shi, Y.R., and Guo, F., 2008, Geochronology and geochemistry of the Hegenshan ophiolitic complex: implications for late-stage tectonic evolution of the Inner Mongolia–Daxinganling Orogenic Belt, China. Journal of Asian Earth Sciences, 32, 348–370.

Murphy, J.B., 2013, Appinite suites: a record of the role of water in the genesis, transport, emplacement and crystallization of magma. Earth-Science Reviews, 119, 35–59.

Norrish, K. and Hutton, J.T., 1969, An accurate X-ray spectrographic method for the analysis of a wide range of geological samples. Geochimica et Cosmochimica Acta, 33, 431–453.

Rickwood, P.C., 1989, Boundary lines within petrologic diagrams which use oxides of major and minor elements. Lithos, 22, 247–263.

Saunders, A.D., Norry, M.J., and Tarney, J., 1991, Fluid influence on the trace element compositions of subduction zone magma. Philosophical Transactions of the Royal Society of London, Series A. Mathematical, Physical and Engineering Sciences, 335, 377–392.

Scherer, E., Munker, C., and Mezger, K., 2001, Calibration of the lutetium-hafnium clock. Science, 293, 683–687.

Sengör, A.M.C., Natal'in, B.A., and Burtman, V.S., 1993, Evolution of the Altaid tectonic collage and Paleozoic crustal growth in Eurasia. Nature, 364, 299–307.

Shao, J.A., 1991, Crust evolution in the middle part of the northern margin of Sino-Korean Plate. Peking University Publishing House, Beijing, 136 p. (in Chinese with English abstract)

Shi, G.H., Miao, L.C., Zhang, F.Q., Jian, P., Fan, W.M., and Liu, D.Y., 2004, Emplacement age and tectonic implications of the Xilinhot A-type granite in Inner Mongolia, China. Chinese Science Bulletin, 49, 723–729.

Sun, S.S. and McDonough, W.F., 1989, Chemical and isotopic systematics of oceanic basalts: implications for mantle composition and processes. In: Saunders, A.D. and Norry, M.J. (eds.), Magmatism in the Ocean Basins. Geological Society, London, Special Publications, 42, p. 313–345. https://doi.org/10.1144/GSL.SP.1989.042.01.19

Tang, K.D., 1990, Tectonic development of Paleozoic fold belts at the north margin of the Sino-Korean craton. Tectonics, 9, 249–260.

Tong, Y., Jahn, B.M., Wang, T., Hong, D.W., Smith, E.I., Sun, M., Gao, J.F., Yang, Q.D., and Huang, W., 2015, Permian alkaline granites in the Erenhot–Hegenshan belt, northern Inner Mongolia, China: model of generation, time of emplacement and regional tectonic significance. Journal of Asian Earth Sciences, 97, 320–336.

Turner, S., Hawkesworth, C., Gallagher, K., Stewart, K., Peate, D., and Mantovani, M., 1996, Mantle plumes, flood basalts, and thermal models for melt generation beneath continents: assessment of a conductive heating model and application to the Paraná. Journal of Geophysical Research: Solid Earth, 101, 11503–11518.

Wang, G.S., Zhou, Z.G., Liu, C.F., Wu, C., Li, H.Y., and Jiang, T., 2019, Tectonic significance of the Late Carboniferous Zhunmubutai ophiolitic mélange from Xi-Ujimqin, Inner Mongolia. Geological Journal, 54, 364–377.

Wang, G.S., Liu, C.F., Pei, W.X., Zhou, Z.G., Li, H.Y., Wu, C., Zhu, Y., and Ye, B.Y., 2018, Geochemistry and zircon U-Pb-Hf isotopes of the granitoids of Qianjinchang pluton in the Xi Ujimqi, Inner Mongolia: implications for petrogenesis and geodynamic setting. Geological Journal, 53, 767–787.

Wang, Q., 1986, Recognition of the suture between the Sino-Korean and Siberian paleoplates in the middle part of Inner Mongolia. Acta Geological Sinica, 1, 31–43. (in Chinese with English abstract)

Wang, Y.J. and Fan, Z.Y., 1997, Discovery of Permian radiolarians in ophiolite belt on northern side of Xarmoron River, Nei Monggol and its geological significance. Acta Palaeontologica Sinica, 36, 58–69. (in Chinese with English abstract)

Wang, Y.Y., Zeng, L.S., Chen, F.K., Cai, J.H., Yan, G.H., Hou, K.J., and Qang, Q., 2017, The evolution of high Ba-Sr granitoid magmatism from "crust-mantle" interaction: a record from the Laoshan and Huyanshan complexes in the central North China Cration. Acta Petrologica Sinica, 33, 3873–3896. (in Chinese with English abstract)

Windley, B.F., Alexeiev, D., Xiao, W.J., Kröner, A., and Badarch, G., 2007, Tectonic models for accretion of the Central Asian Orogenic Belt. Journal of the Geological Society, 164, 31–47.

Wu, F.Y., Wilde, S.A., Zhang, G.L., and Sun, D.Y., 2004, Geochronology and petrogenesis of the post-orogenic Cu-Ni sulfide-bearing mafic-ultramafic complexes in Jilin Province, NE China. Journal of Asian Earth Sciences, 23, 781–797.

Wu, F.Y., Yang, J.H., Wilde, S.A., and Zhang, X.O., 2005, Geochronol-

ogy, petrogenesis and tectonic implications of Jurassic granites in the Liaodong Peninsula, NE China. Chemical Geology, 221, 127–156.

Wu, F.Y., Jahn, B.M., Wilde, S.A., Lo, C.H., Yui, T.F., Lin, Q., Ge, W.C., and Sun, D.Y., 2003, Highly fractionated I-type granites in NE China (II): isotopic geochemistry and implications for crustal growth in the Phanerozoic. Lithos, 67, 191–204.

Xiao, W.J., Windley, B.F., Hao, J., and Zhai, M.G., 2003, Accretion leading to collision and the Permian Solonker suture, Inner Mongolia, China: termination of the central Asian orogenic belt. Tectonics, 22, 1069.

Xiao, W.J., Windley, B.F., Huang, B.C., Han, C.M., Yuan, C., Chen, H.L., Sun, M., Sun, S., and Li, J.Y., 2009, End-Permian to mid-Triassic termination of the accretionary processes of the southern Altaids: implications for the geodynamic evolution, Phanerozoic continental growth, and metallogeny of Central Asia. International Journal of Earth Sciences, 98, 1189–1217.

Xiao, W.J., Windley, B.F., Sun, S., Li, J.L., Huang, B.C., Han, C.M., Yuan, C., Sun, M., and Chen, H.L., 2015, A tale of amalgamation of three Permo-Triassic collage systems in central Asia: oroclines, sutures, and terminal accretion. Annual Review of Earth and Planetary Sciences, 43, 477–507. https://doi.org/10.1146/annurev-earth-060614-105254

Xiong, F.H., Ma, C.Q., Wu, L., Jiang, H.A., and Liu, B., 2015, Geochemistry, zircon U-Pb ages and Sr-Nd-Hf isotopes of an Ordovician appinitic pluton in the East Kunlun orogen: new evidence for Proto-Tethyan subduction. Journal of Asian Earth Sciences, 111, 681–697.

Xu, B. and Chen, B., 1997, Framework and evolution of the middle Paleozoic orogenic belt between Siberian and North China Plates in northern Inner Mongolia. Science in China, 40, 463–469.

Xu, B., Charvet, J., Chen, Y., Zhao, P., and Shi, G.Z., 2013, Middle Paleozoic convergent orogenic belts in western Inner Mongolia (China): framework, kinematics, geochronology and implications for tectonic evolution of the Central Asian Orogenic Belt. Gondwana Research, 23, 1242–1364.

Xu, Y.S., 1986, Complex rocks of Indo-China episode from Luotuochang, Zhaomeng, area, Inner Mongolia, China. Science Bulletin, 31, 761–764.

Yang, J., Zhang, Z., Chen, Y., Yu, H., and Qian, X., 2017, Ages and origin of felsic rocks from the eastern Erenhot ophiolitic complex, southeastern Central Asian Orogenic Belt, Inner Mongolia China. Journal of Asian Earth Sciences, 144, 126–140.

Yuan, L.L., Zhang, X.H., Zhai, M.G., and Xue, H.M., 2016, Petrogenesis and geodynamic implications of appinite suit. Acta Petrologica Sinica, 32, 1556–1570. (in Chinese with English abstract)

Zhang, J.R., Wei, C.J., Chu, H., and Chen, Y.P., 2016, Mesozoic metamorphism and its tectonic implication along the Solonker suture zone in central Inner Mongolia, China. Lithos, 261, 262–272.

Zhang, L.C., Ying, J.F., Chen, Z.G., Wu, H.Y., Wang, F., and Zhou, X.H., 2008, Age and tectonic setting of Triassic basic volcanic rocks in southern Da Hinggan Range. Acta Petrologica Sinica, 24, 911–920. (in Chinese with English abstract)

Zhang, S.H., Zhao, Y., Ye, H., Liu, J.M., and Hu, Z.C., 2014, Origin and evolution of the Bainaimiao arc belt: implications for crustal growth in the southern Central Asian orogenic belt. Geological Society of America Bulletin, 126, 1275–1300.

Zhang, X.H., Wilde, S.A., Zhang, H.F., and Zhai, M.G., 2011, Early Permian high-K calc-alkaline volcanic rocks from NW Inner Mongolia, North China: geochemistry, origin and tectonic implications. Journal of the Geological Society, 168, 525–543.

Zhang, X.H., Gao, Y.L., Wang, Z.J., Liu, H., and Ma, Y.G., 2012a, Carboniferous appinitic intrusions from the northern North China craton: geochemistry, petrogenesis and tectonic implications. Journal of the Geological Society, 169, 337–351.

Zhang, X.H., Xue, F.H., Yuan, L.L., Ma, Y.G., and Wilde, S.A., 2012b, Late Permian appinite-granite complex from northwestern Liaoning, North China Craton: petrogenesis and tectonic implications. Lithos, 155, 201–217.

Zhang, X.H., Yuan, L.L., Xue, F.H., Yan, X., and Mao, Q., 2015, Early Permian A-type granites from central Inner Mongolia, North China: magmatic tracer of post-collisional tectonics and oceanic crustal recycling. Gondwana Research, 28, 311–327.

Zhang, X.H., Zhang, H.F., Tang, Y.J., Wilde, S.A., and Hu, Z.C., 2008, Geochemistry of Permian bimodal volcanic rocks from central Inner Mongolia, North China: implication for tectonic setting and Phanerozoic continental growth in Central Asian Orogenic Belt. Chemical Geology, 249, 262–281.

Zhang, Z.C., Chen, Y., Li, K., Li, J.F., Yang, J.F., and Qian, X.Y., 2017, Geochronology and geochemistry of Permian bimodal volcanic rocks from central Inner Mongolia, China: implications for the late Palaeozoic tectonic evolution of the south-eastern Central Asian Orogenic Belt. Journal of Asian Earth Sciences, 135, 370–389.

Zhao, P., Xu, B., and Zhang, C.H., 2017, A rift system in southeastern Central Asian Orogenic Belt: constraint from sedimentological, geochronological and geochemical investigations of the late Carboniferous–early Permian strata in northern Inner Mongolia (China). Gondwana Research, 47, 342–357.

Zhao, P., Jahn, B.M., Xu, B., Liao, W., and Wang, Y.Y., 2016a, Geochemistry, geochronology and zircon Hf isotopic study of peralkaline-alkaline intrusions along the northern margin of the North China Craton and its tectonic implication for the southeastern Central Asian Orogenic Belt. Lithos, 261, 92–108.

Zhao, P., Xu, B., Tong, Q.L., Chen, Y., and Faure, M., 2016b, Sedimentological and geochronological constraints on the Carboniferous evolution of central Inner Mongolia, southeastern Central Asian Orogenic Belt: inland sea deposition in a post-orogenic setting. Gondwana Research, 31, 253–270.

Zhong, Y.F., Ma, C.Q., Liu, L., Zhao, J.H., Zheng, J.P., Nong, J.N., and Zhang, Z.J., 2014, Ordovician appinites in the Wugongshan Domian of the Cathaysia Block, South China: geochronological and geochemical evidence for intrusion into a local extensional zone within an intracontinental regime. Lithos, 198–199, 202–216.

Zhu, J.B. and He, Z.J., 2017, Detrital zircon records of upper Permian–middle Triassic sedimentary sequence in the Linxi area, Inner Mongolia and constraints on timing of final closure of the Paleo-Asian Ocean (eastern segment). Acta Geologica Sinica, 91, 232–248. (in Chinese with English abstract)